EFDA Task TW6-TPDS-DIADEV deliverable 2: ITER Fast Ion Collective Scattering Development of diagnostic components and techniques

Michelsen, S.; Bindslev, Henrik; Korsholm, Søren Bang; Leipold, Frank; Meo, Fernando; Michelsen, Poul; Nielsen, Anders Henry; Tsakadze, Erekle

Publication date:
2009

Document Version
Publisher's PDF, also known as Version of record

EFDA Task TW6-TPDS-DIADEV deliverable 2: ITER Fast Ion Collective Scattering Development of diagnostic components and techniques

Risø-R-Report

S. Michelsen, H. Bindslev, S. B. Korsholm, F. Leipold, F. Meo,
P.K. Michelsen, A.H. Nielsen, Erekle Tsakadze
Risø-R-1716(EN)
December 2009

Risø DTU
National Laboratory for Sustainable Energy

Author: S. Michelsen, H. Bindslev, S. B. Korsholm, F. Leipold, F. Meo, P.K. Michelsen, A.H. Nielsen, Erekle Tsakadze
Title: EFDA Task TW6-TPDS-DIADEV deliverable 2: ITER Fast Ion Collective Scattering Development of diagnostic components and techniques
Division: Plasma Physics and Technology Programme

Abstract (max. 2000 char.):
In 2003 the Risø CTS group finished a feasibility study and a conceptual design of an ITER fast ion collective Thomson scattering system. The purpose of the CTS diagnostic is to measure the distribution function of fast ions in the plasma with particular interest in fusion alphas. The feasibility study demonstrated that the only system, which can fully meet the ITER measurement requirements for confined fusion alphas, is a 60 GHz system. The study showed that by using two powerful microwave sources (gyrotrons) of this frequency both on the low field side, and two antenna systems, one on the low field side and one on the high field side, it is possible to resolve the distribution function of fast ions both for perpendicular and parallel velocities with good spatial and temporal resolution. The present work concerned a continuation of this work, and the following tasks were performed. 1) Optimisation of the design, considering the scattering geometries, variations in plasma profiles, magnetic equilibria etc. 2) Development of numerical codes for determination of the geometry of the antenna system on the high field side, including shapes and positions of mirrors and receiver horns. 3) A model experiment was set up in order to test and support the theoretical and numerical results. From the design studies various R&D issues critical to the viability of the CTS diagnostic on ITER were identified; the most urgent ones are addressed in the presented R&D tasks.

Risø-R-1716(EN)
December 2009

ISSN 0106-2840
ISBN 978-87-550-3792-2

Contract no.:
EFDA Task TW6-TPDS-DIADEV deliverable 2
FU06-CT-2005-00357

Group's own reg. no.:
1710019-26

Sponsorship:

Cover :

Pages: 42
Tables: 0
References: 2

Information Service Department
Risø National Laboratory for Sustainable Energy
Technical University of Denmark
P.O.Box 49
DK-4000 Roskilde
Denmark
Telephone +45 46774005
bibl@risoe.dtu.dk
Fax +45 46774013
www.risoe.dtu.dk

1 Introduction

In 2003 the Risø CTS group finished a feasibility study and a conceptual design of an ITER fast ion collective Thomson scattering system (Contract 01.654, Ref. 1). The purpose of the CTS diagnostic is to measure the distribution function of fast ions in the plasma with particular interest in fusion alphas. The feasibility study demonstrated that the only system, which can fully meet the ITER measurement requirements for confined fusion alphas, is a 60 GHz system. The study showed that by using two powerful microwave sources (gyrotrons) of this frequency both on the low field side, and two antenna systems, one on the low field side and one on the high field side, it is possible to resolve the distribution function of fast ions both for perpendicular and parallel velocities with good spatial and temporal resolution.

The EFDA Contract 04-1213 (Ref. 2) with Risø National Laboratory concerned a continuation of this work, and the following tasks were performed.

- Optimisation of the design, considering the scattering geometries, variations in plasma profiles, magnetic equilibria etc.
- Development of numerical codes for determination of the geometry of the antenna system on the high field side, including shapes and positions of mirrors and receiver horns.
- A model experiment was set up in order to test and support the theoretical and numerical results.

From the design studies various R&D issues critical to the viability of the CTS diagnostic on ITER were identified; the most urgent ones are addressed in the presented R&D tasks.

In the following the three deliverables are presented followed by sections describing the performed investigations.

2 Deliverable (i)

Initiate the development of codes for model calculations to optimize mirrors. This is non-trivial since 8 or 10 beams are to be transmitted on the same mirror. In addition, a physics feasibility study has shown that ellipsoidal beams are needed to satisfy the ITER measurement requirements for fast-alpha measurements. The codes developed should therefore be able to calculate mirror shapes for such beams in three dimensions

.

2.1 Introduction

Calculation of the transmission of the scattered beam from the plasma to the receiving microwave horn may be performed assuming that the beam at the horn is known. When this is the case it is in principle possible to calculate the beam parameters in the plasma. The optimization process is then to find the best positions and shapes of the mirrors in the system. The Gaussian beam approximation is sufficient as long as the beam spreading is not too large. For the CTS antenna system on the high field side the beam has to pass through a slot of limited height in the blanket module. When the height of the slot is of the order of a few wavelengths, the slot is acting as a waveguide and the Gaussian beam approximation may break down in the vertical direction.

2.1.1 Finite difference code

It has been found that a detailed full three-dimensional numerical simulation of the electromagnetic wave transmission is not possible even without including the propagation in the plasma, because for the wavelength in question significantly more grid points are needed than can be handled on present-day computers. However a two-dimensional code has been developed in order to obtain some general information about the wave propagation through the slot. Furthermore, the code may help to find the best coupling from the Gaussian beam to the waveguide propagation in the slot, and the calculations may also be tested against the measurements with the mock-up model.

2.1.2 New code for Gaussian beam calculation

A new code for astigmatic Gaussian beam propagation has been developed. This code is combined with a new code for calculation of optimized mirror shapes. The codes have been used to find two and four mirror solutions, which satisfy the geometrical constraints. Some results of these calculations are presented in section 4.2.

2.2 ITER blanket cut-out calculations.

In order to study the transmission through the slot in details, a numerical scheme has been developed, a so-called Computational Electro-Magnetic (CEM), in which Maxwell equations are solve directly in a two-dimensional geometry. The CEM code has been improved from the one used in Ref. 2. In that work the surface and especially the normal to the surface was calculated from the numerical values, using the underlying grid. This approach has proved to be too inaccurate and has been replaced by a method using analytical expressions. In CEM calculations the starting

point is an input field calculated without the blanket present. The boundary conditions ($\hat{n}x\vec{E}_{tot} = 0$) are then applied to get the total field when the blankets are present.
Some results of the CEM calculations of the slot between the HFS blankets are shown below. Changes of the radius of curvature of the blanket (R), the slot height (h_s), the vertical offset (Δ) and the tilt of the incident beam (θ) have been investigated. The beam is tilted around the beam waist position, which is placed at the entrance of the slot. In the simulations presented below only one parameter is changed at a time. For each case the Pointing vector: $\vec{S} = \vec{E}x\vec{H}^*$ is calculated. It represents the energy flux in a given point.

2.2.1 Parameters

In the CEM calculations the following parameters have been used:

Beam width at the beam waist (W_0)	= $0.64*h_s$
Beam waist position (Z_0)	= -15*λ (measured from the centre)
Damping (PML) layer	= 3*λ
Free space to the left of the blanket	= 10*λ
Free space to the right of the blanket	= 20*λ
Resolution in the vertical direction	= 10 points /λ
Blanket length	= 20*λ

To couple a beam optimal to a waveguide a beam width of 0.64*h is used. The same beam size is used in these calculations. The beam waist position is placed at the entrance to the slot.

2.2.2 Resolution studies

Numerical modelling of electromagnetic wave propagation in large systems requires a very high resolution in order to give correct results. This is illustrated in Figure 1, where an incoming field displaced vertically Δ = 25 mm from the slot with h_s= 3*λ, is considered. In this case the field should not be transmitted to the other side of the blanket due to total back reflection, no field should enter the blanket, and there should be zero field on the other side. It is seen that if the resolution is poor the field is not cancelled on the right side of the blanket.

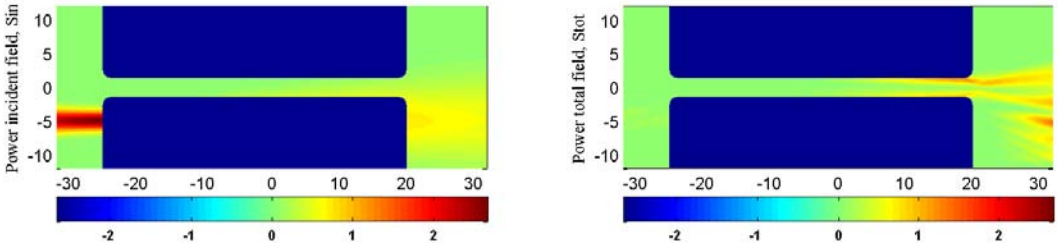

Figure 1. Power of a) the incident field and b) the total field for R=1* λ, h_s=3* λ, θ=0^0. Blanket length=45*λ.

When the blanket length is increased the resolution per wavelength also has to be increased in order to keep errors limited as illustrated on Figure 2 a) and b) for a blanket lengths of 20*λ and 45*λ, respectively. When there is total reflection there is zero flow and the Pointing vector is zero. The input field (shown in blue) only shows the field visible on Figure 1a.
It can also be noted that the error inside the blanket is larger for a long blanket than for a short. In the following calculations a short blanket (20*λ) with an average of 18.5 points per wavelength will be used to get reliable results.

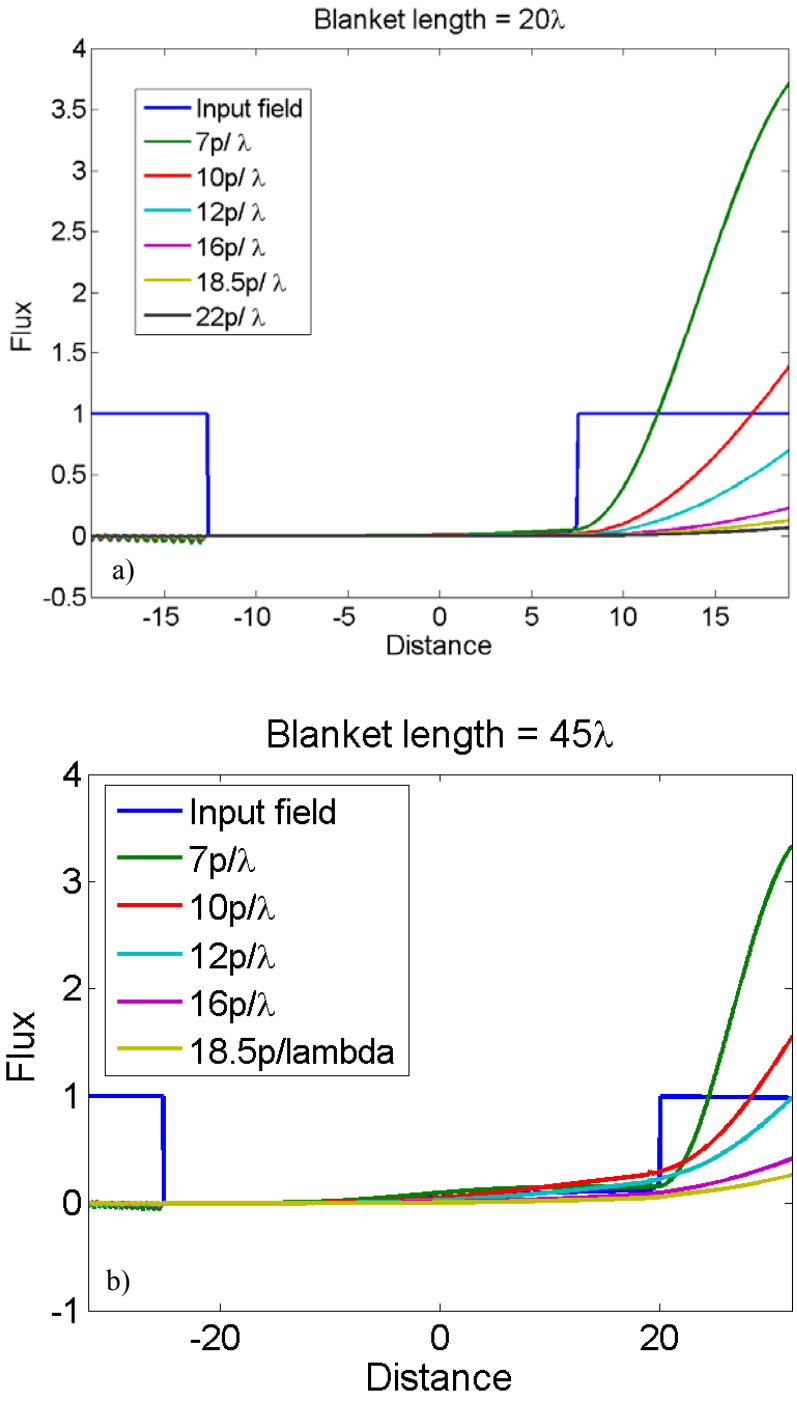

Figure 2. Flux crossing a vertical line as a function of horizontal distance for R=1* λ, h_s=3* λ, θ=0^0. a) Blanket length=20*λ, and b) Blanket length =45*λ.

2.2.3 Radius of curvature (R)

In the location of the HFS receiver it may be an option to change the edges of the blanket cut-out. To investigate the influence of the radius of curvature of the blanket edges, the radius of curvature is changed from 0* λ to 4* λ, with θ=0˚ and Δ=0 mm. Figure 3 shows the power of the Poynting vector for R=1* λ and 3* λ and a slot height of 6* λ.

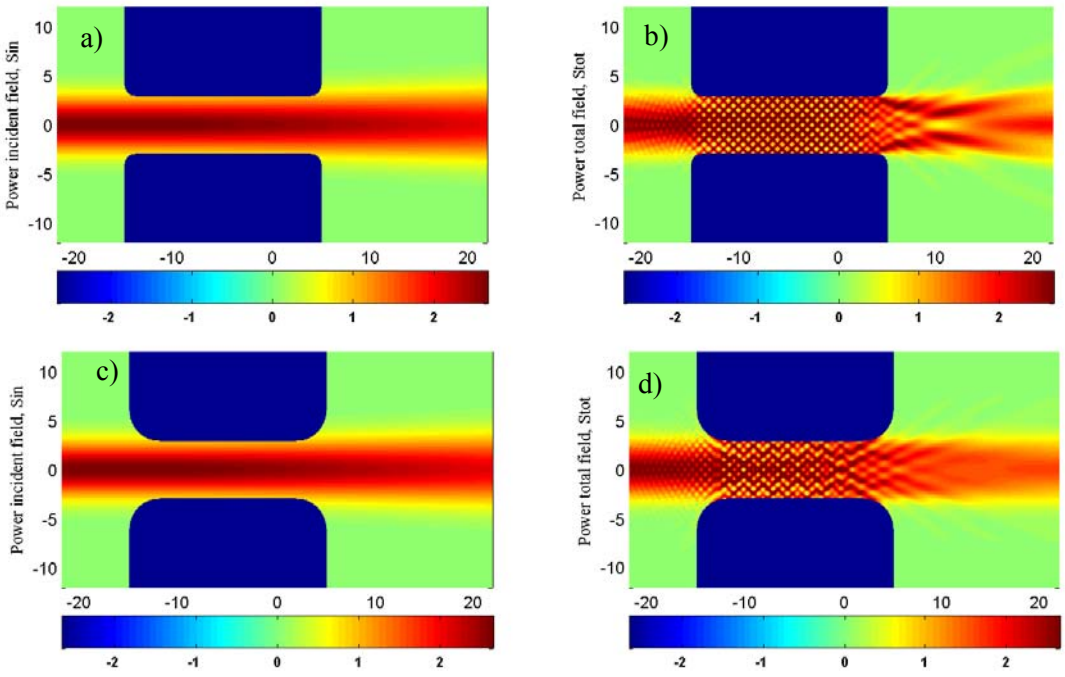

Figure 3. Power of the incident field a) R=1 * λ and c) R=3* λ. Total field for b) R=1* λ and d) R=3* λ. Blanket length=20*λ and h_s=6* λ, θ=0^0

The first column shows the power of the input field. It is calculated without the blanket present, but it is shown together with the blanket for illustration purposes. The second column shows the total field power with all reflections when the blanket is present. It is seen that the curvature of the blanket has an influence on the transmitted beam.

The cross section of the input field power is shown in Figure 4 a) and b) for h_s=3* λ and h_s=6* λ respectively. The total field before the blanket is shown in c) h_s=3* λ and d) h_s=6* λ. The total field after the blanket is shown in e) h_s=3* λ and f) h_s=6* λ at the distance of 20λ.The graphs have been displaced 0.5 for increasing radius of curvature, to show the difference in the transmitted field in a more clear way. The results have a contribution from the radius of curvature but it might also depend on the blanket length, which is short, due to the mentioned resolution problems. Note that when the distance from the blanket is increased the near field contributions will disappear and there is one peak. Due to lack of computer power it was not possible to make calculations with larger distance after the blankets.

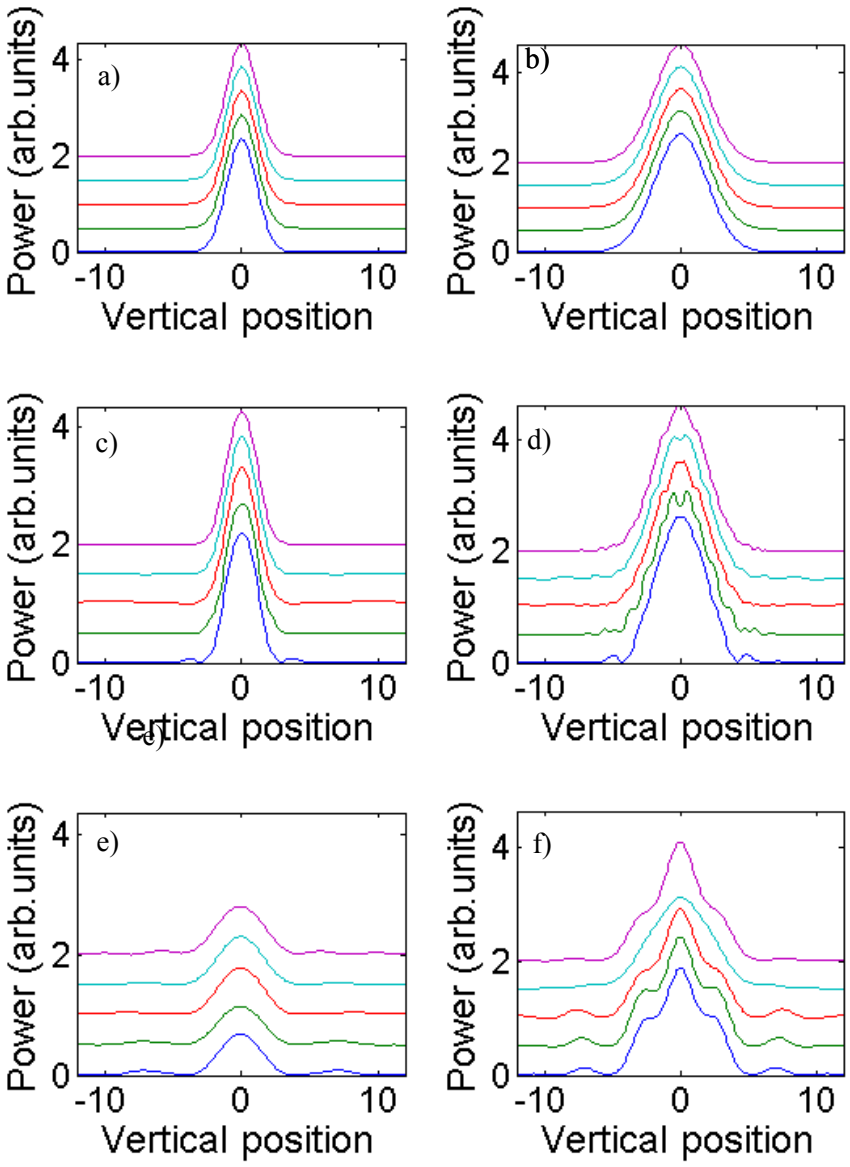

Figure 4. Cross section of the power distribution as a function of radius of curvature. Input field: a) h_s =3* λ and b) h_s =6* λ. The total field entering the blanket: c) h_s =3* λ and d) h_s =6* λ. The total field leaving the blanket: d) h_s =3* λ and f) h_s =6* λ. The colour codes are: R=0*λ (blue), R=1*λ (green), R=2*λ (red), R=3*λ (light blue) and R=4*λ (purple). θ=0 and Δ=0.The curves are displaced by R/λ*0.5.

To get an impression about how much power is transmitted, the energy flux crossing a circular line with radius of 5*λ and centre in the middle of the slot at both side of the blanket is calculated as illustrated in Figure 5. The value for the total field leaving the blanket is divided with the valued for the input field. This is defined as the transmission and shown in Figure 6. It is seen that the radius does not affect the transmission significantly. It is also seen that the largest h_s has the highest transmission.

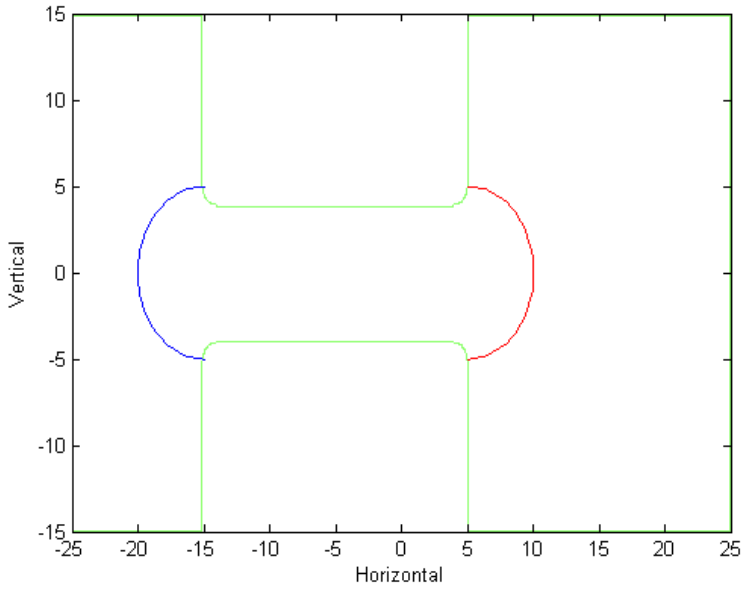

Figure 5. Illustration of the boundary on the blanket (green), the circles for calculation of the flux before (blue) and after the blanket (red).

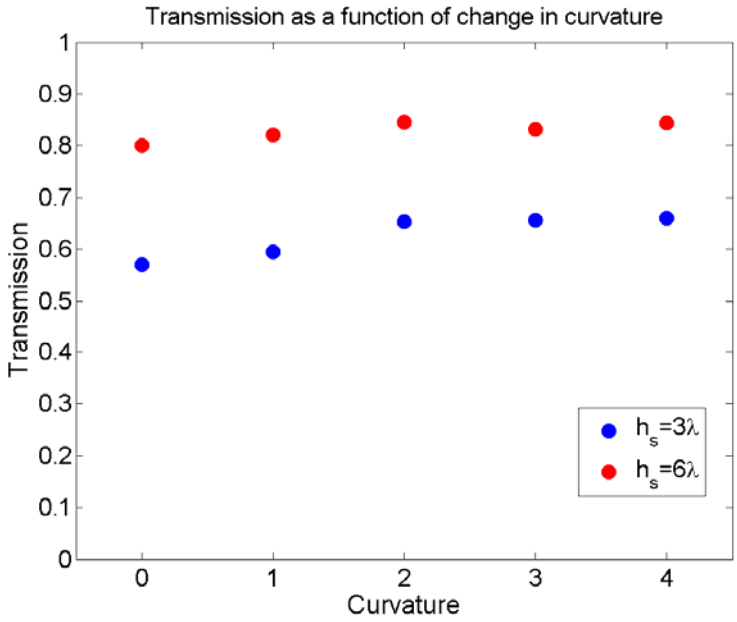

Figure 6. Transmission as a function of radius of curvature (in units of λ), for h_s = 3* λ and h_s =6* λ, θ=0^0, Δ=0.

The following simulations have been performed when both shapes of the entrance and exit slit have been changed. The plasma facing end of the blanket will most likely not be modified; hence studies are done on the influence of the slot entrance shape in the following.

2.2.4 Slot height (h_s)

As already illustrated in the previous figures the slot height has a significant influence on the transmitted beam. Figure 7 shows the incident and total power for two different slot heights using a beam width of $0.64*h_s$. Please note that in this case the input power will thus increase with increasing slot height. From Figure 7b it can be observed that there is a reflection from the entrance of the blanket and a smaller beam is transmitted on the other side. Figure 7d shows the case for the large slot, where the reflection pattern inside the slot is more distinct.

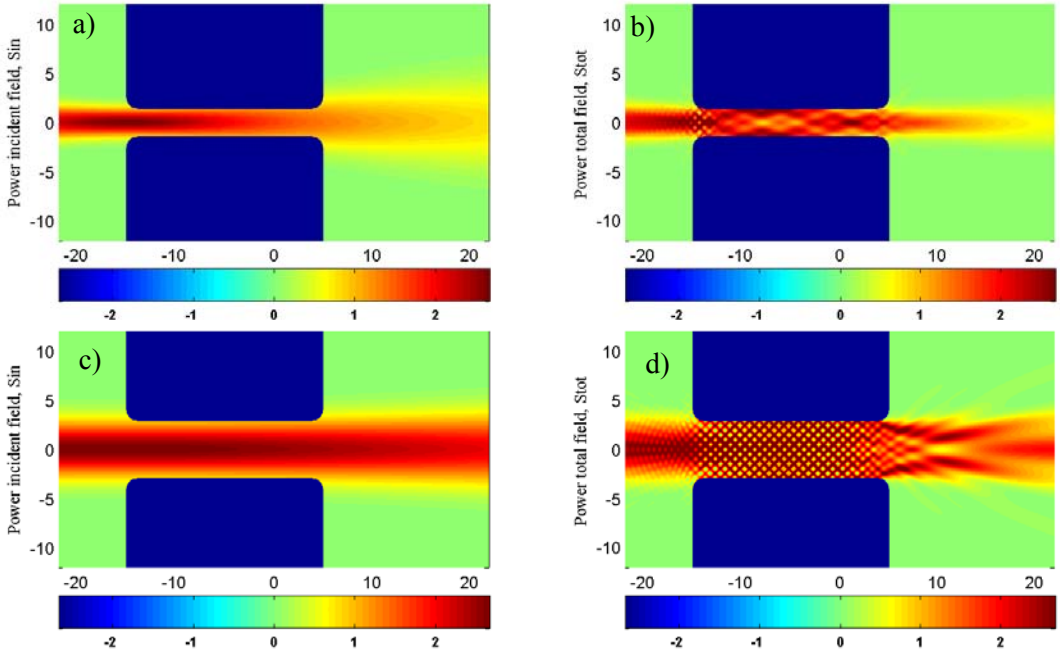

Figure 7. Power for the input field: a) $h_s = 3*\lambda$ and c) $h_s = 6*\lambda$; total field: $h_s = 3*\lambda$ and d) $h_s = 6*\lambda$.

It is clearly seen in Figure 8 that the reflection pattern becomes more pronounced with increasing slot height. The slot height has a large influence on the total field after the blanket. It may be noted that a larger h_s in this case means a broader beam and thus a smaller vertical divergence angle resulting in the input field having significant reflection in the whole slot, whereas a narrow beam will only reflect near the entry. Note that only one main peak was observed in the experimental measurements performed in Ref. 2. In these reported experiments the slot height was changed between $4*\lambda$ and $6*\lambda$. It is important to note that these experiments were measuring the far field where these near field effects become washed out.

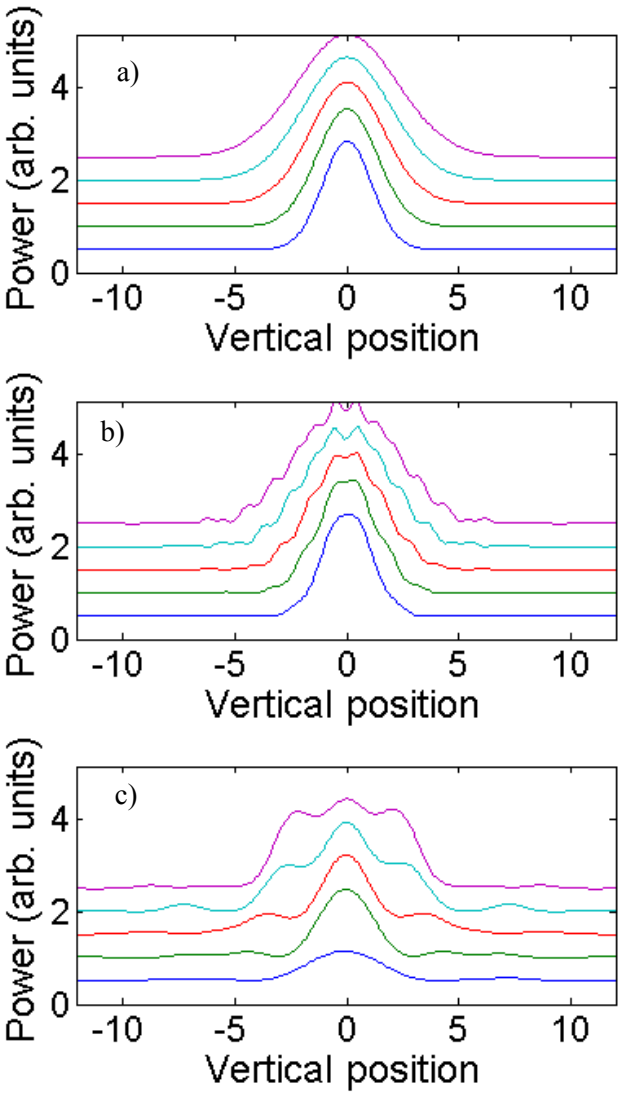

Figure 8. Cross section of the power as a function of slot height for a) input field, b) total field before the blanket and c) total field after the blanket. $h_s = 3 * \lambda$ (blue), $h_s = 4 * \lambda$ (green), $h_s = 5 * \lambda$ (red), $h_s = 6 * \lambda$ (light blue), $h_s = 7 * \lambda$ (purple).

The transmission is shown in Figure 9, and it can be seen that the transmission decreases as the slot height is lowered. Furthermore, the narrow slot has a larger divergence angle, which will decrease the effective CTS signal coming from scattering volume in the central part of the possible measuring area.

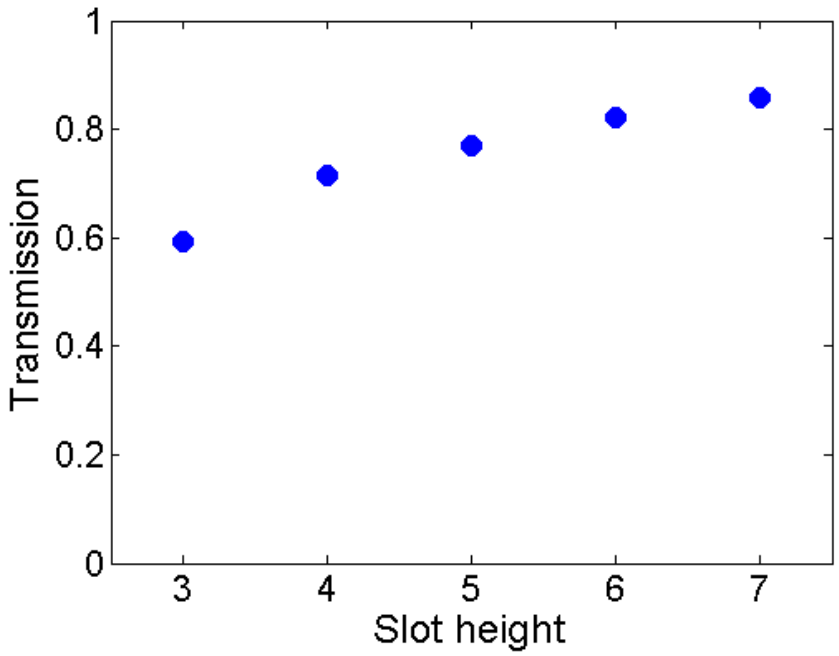

Figure 9. Transmission as a function of slot height (units of λ), R= 5, θ=0 and Δ=0;

The antenna mirror system will be designed in order to optimize the transmission of a beam with a chosen size. If a blanket module is misaligned this will have an effect on the transmission. For a fixed input field and for varying slot height the results illustrated in Figure 10 are obtained. It is seen that when the beam is larger than the slot height there are large reflections and the transmitted beam is lower and narrower (as seen for $h_s=3*\lambda$). When the slot height is larger than the beam, more power will be transmitted (as shown for $h_s=8*\lambda$). When the slot height becomes too high the beam converts into higher order modes in the slot.

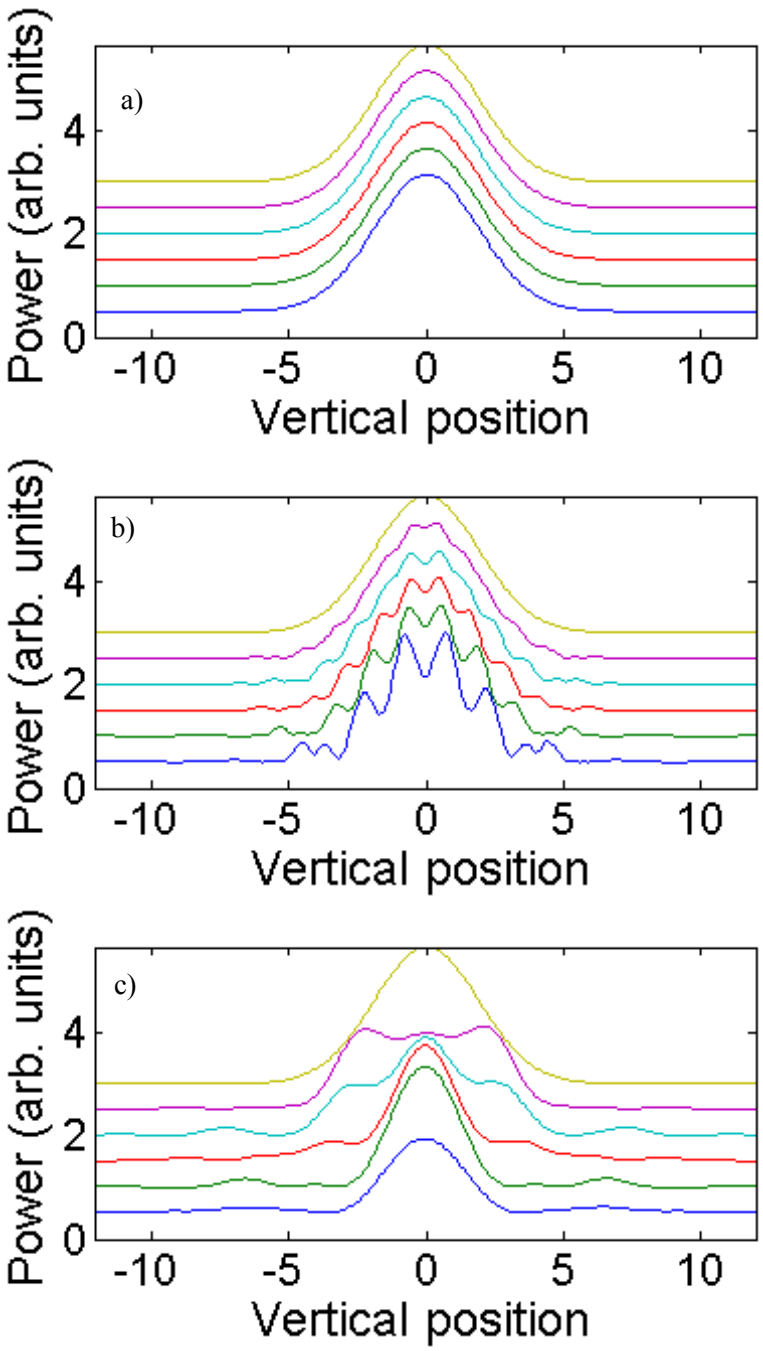

Figure 10. Cross section of the power as a function of slot height for fixed W_0=3.8*λ . a) input field, b) total field before the blanket and c) total field after the blanket. h_s =3* λ (blue), h_s =4* λ (green), h_s =5* λ (red), h_s =6* λ (light blue), h_s =7* λ (purple) and h_s =8* λ (yellow)

2.2.5 Vertical offset (Δ).

One parameter which is important with respect to aligning the system at ITER is the vertical offset of the beam. This is illustrated on Figure 11 which shows the power for Δ = 5 mm, 15 mm and 25 mm and for h_s=3*λ. Note that when there is total back reflection there is no flux and therefore no visible beam as seen on Figure 11 d) for the 25 mm offset. The small slot height is used in order to make the offset effect more clear. It is seen that the offset can have a large influence on the beam quality, even that a large fraction of the beam is transmitted through the slot. It is seen on (d) that when the beam is offset by 25 mm, there is still a very small fraction of power on the right side, which is due to the error accumulated through the system as mentioned in the beginning of the section.

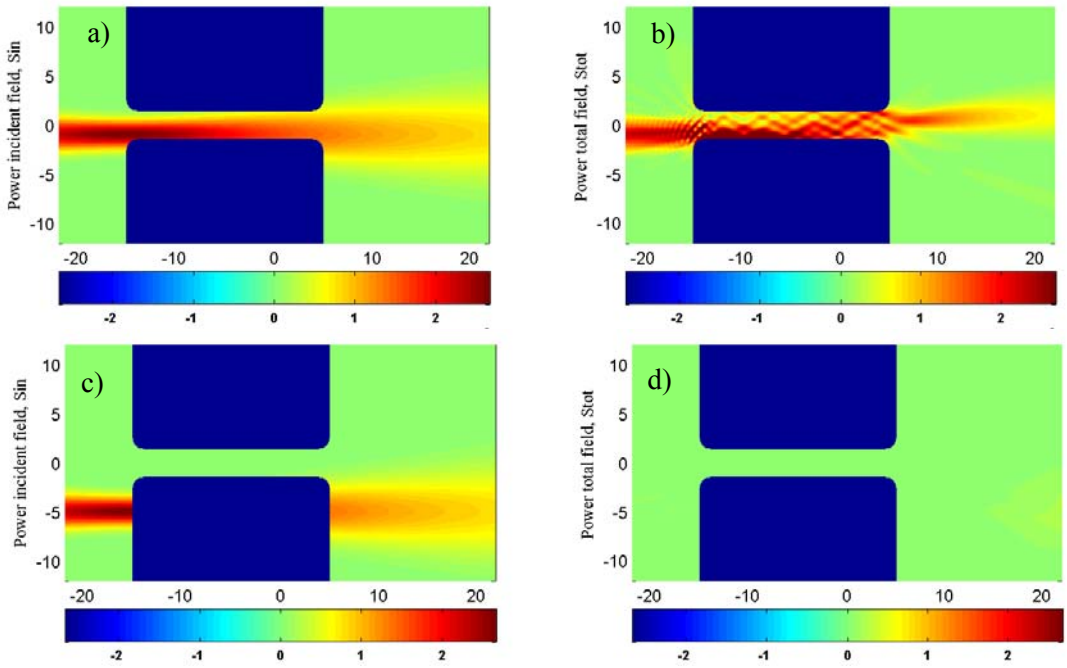

Figure 11. Power for different vertical offset, Δ=5 mm: a) input and b) total field, and Δ=15 mm: c) input and d) total field. R=1*λ, θ=0 and h_s=3*λ

Figure 12 shows the power cross section, and it is seen that the Δ should be below 5 mm to get a centred beam through the slot. Here the reflection on the front of the blanket is clearly seen as the ripples on the beam. When the signal is almost zero there is no transport of power, i.e. the beam is reflected straight back.

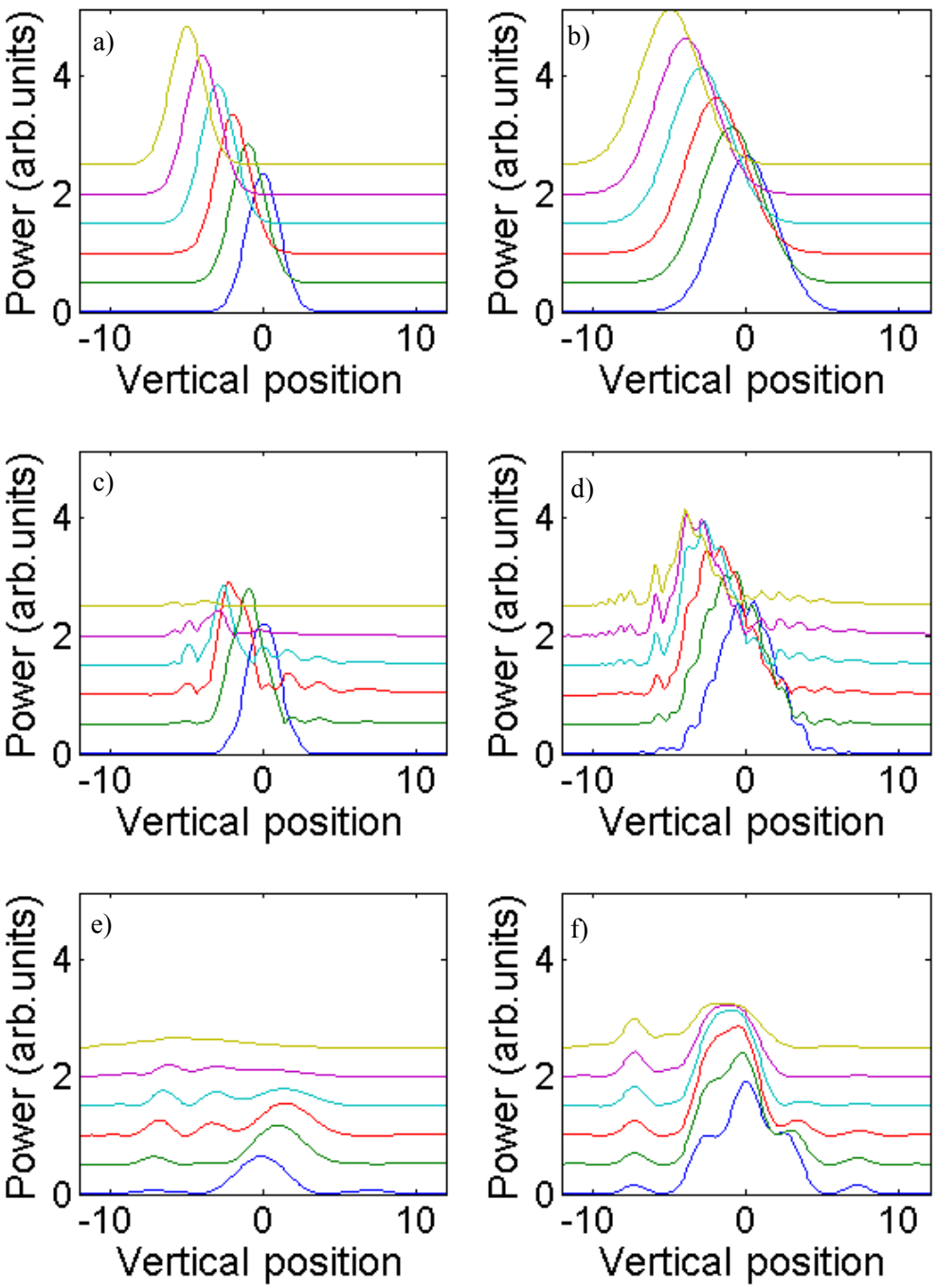

Figure 12 Cross section of the power as a function of vertical offset. Input field: a) $h_s=3*\lambda$ and b) $h_s=6*\lambda$. Total field before the blanket: c) $h_s=3*\lambda$ and d) $h_s=6*\lambda$. Total field after the blanket: e) $h_s=3*\lambda$ and f) $h_s=6*\lambda$. . The colour codes are: Δ=0 mm (blue), Δ=5mm (green), Δ=10 mm (red), Δ=15 mm (light blue), Δ=20 mm (purple), and Δ=25 mm (yellow)

The transmission as a function of Δ is shown in Figure 13. It is seen that transmission is decreasing for increasing Δ, but that a 5 mm misalignment may be tolerable for both cases.

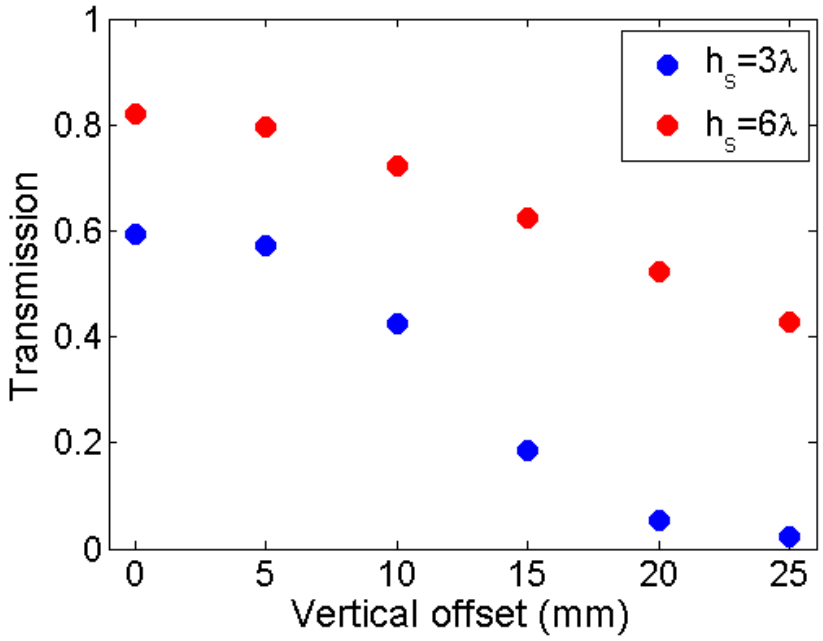

Figure 13. Transmission as a function vertical offset for h_s =3* λ and h_s =6* λ, R= 1* λ and θ=0.

2.2.6 Tilt of the beam (θ)

A misalignment of the antenna system may also cause a tilt of the beam. Figure 14 shows the behaviour when the beam is tilted 2˚,4˚, 6˚ and 20˚ for h_s= 6*λ. It is seen that a small tilt gives rise to reflection on the blanket. When the angle is increased the field has multiple reflections in the slot and the result is distorted from the centre position as seen for the 20° tilt.

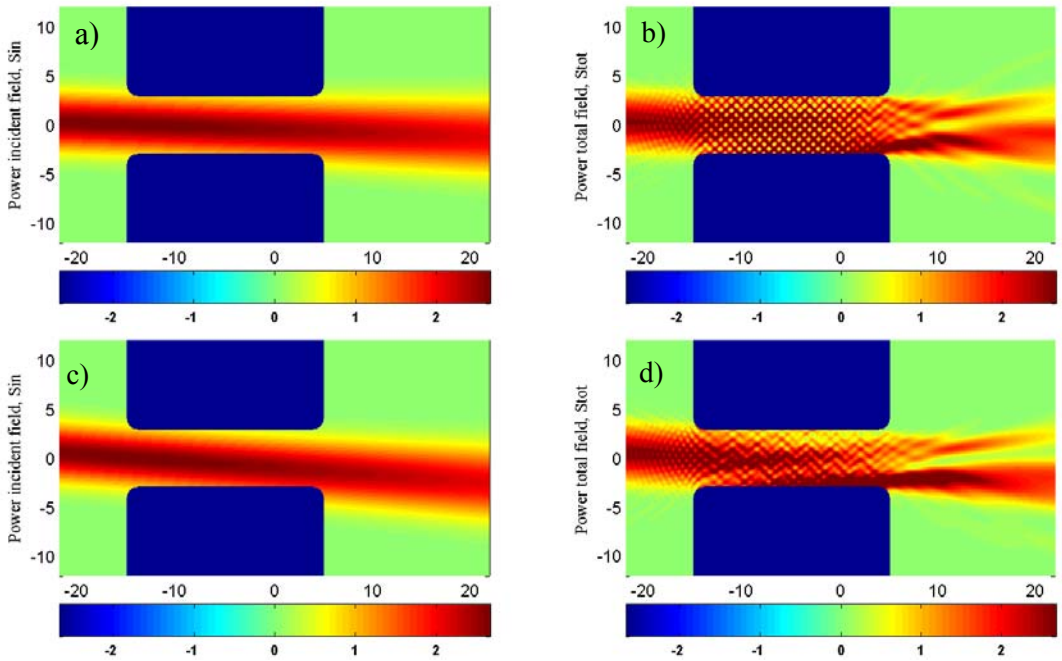

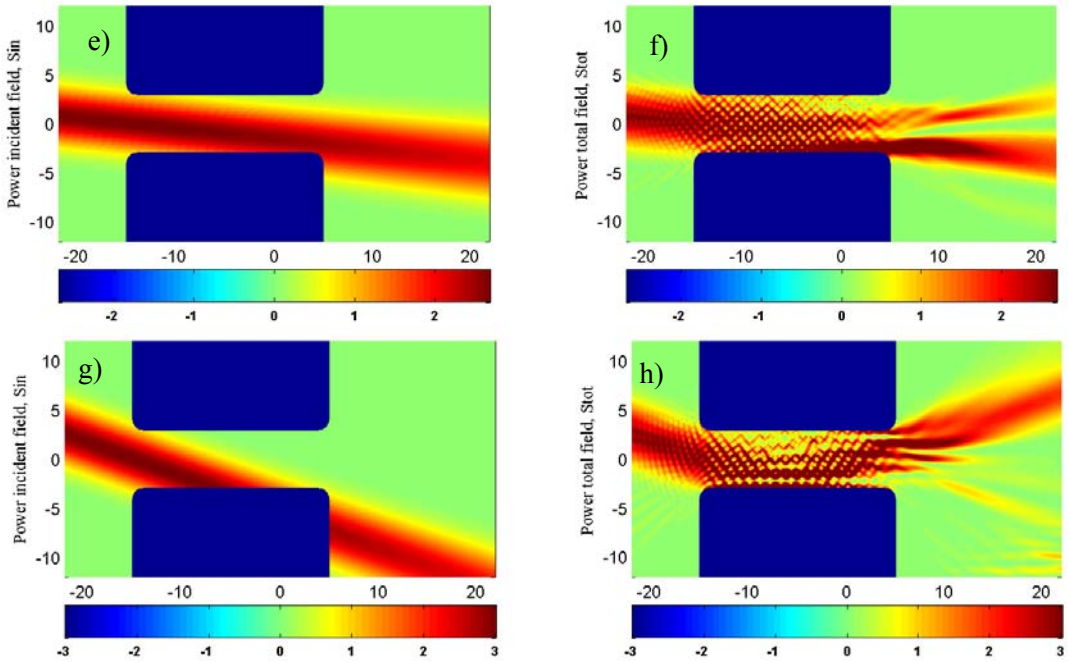

Figure *14*. Power for different tilt angle. θ = 20: a) input and b) total field, θ=40: c) input and d) total field, θ=6^0: c) input and d) total field, θ=20^0, e) input and f) total field. R=1*λ, Δ=0 and h_s=6*λ

This is also seen on Figure 15e) and f) which shows the cross section of the total power after the blanket for h_s=3*λ and h_s=6*λ respectively. Figure 15a) and b) shows the input which looks larger when the angle increases. This is due to the position of the cross section which is aligned with respect to the blanket, and held constant for all graphs. When the tilt becomes too large the transmitted beam has two peaks which will separate even further. This is unacceptable, since the CTS scattering volume should be in the mid plane. Therefore, the study shows that it is essential that the alignment fulfil the requirement that the angle of the beam is kept below 6˚.

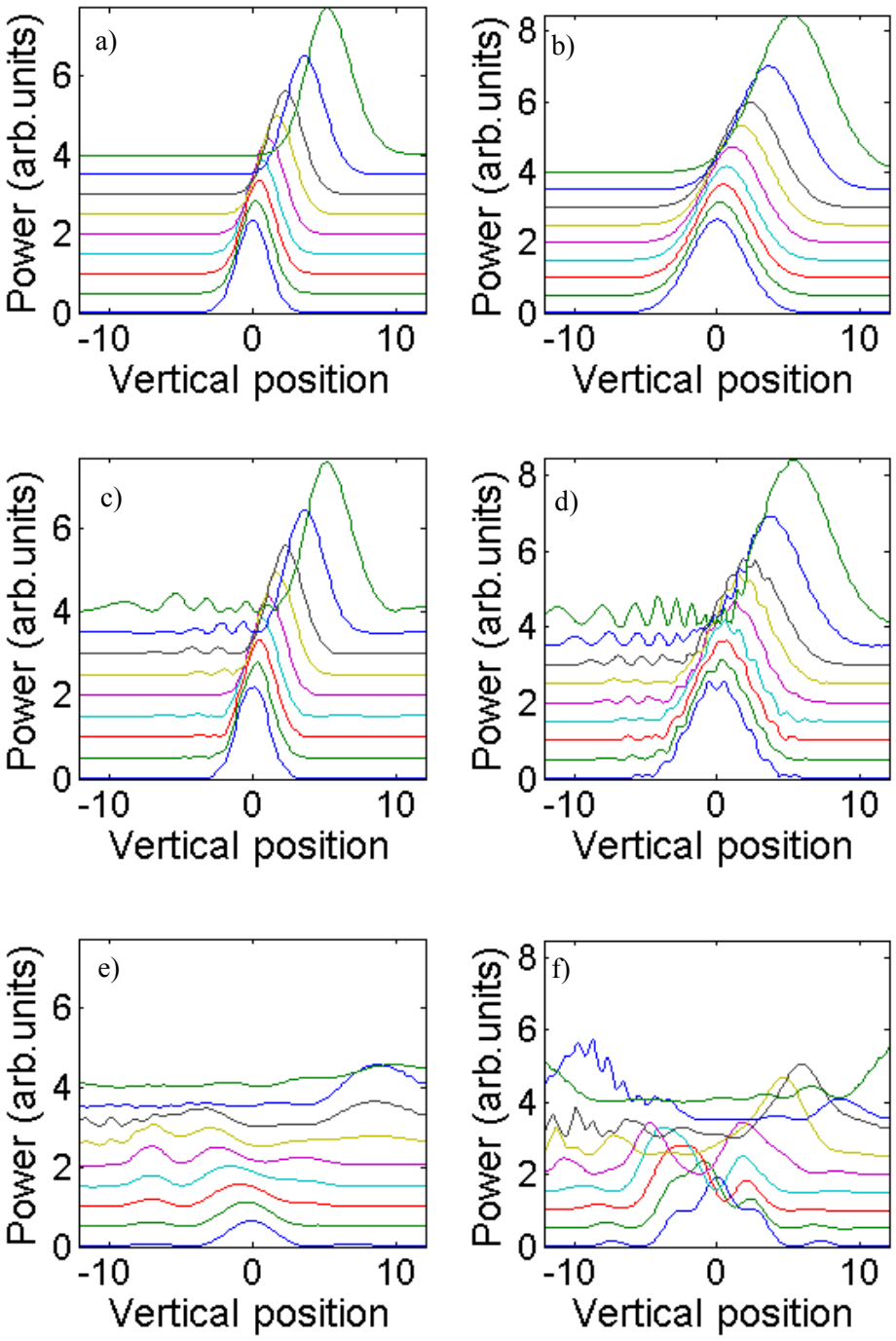

Figure 15 Cross section of the power as a function of tilt. Input field: a) $h_s=3*\lambda$ and b) $h_s=6*\lambda$. Total field before blanket: c) $h_s=3*\lambda$ and d) $h_s=6*\lambda$. Total field after blanket: e) $h_s=3*\lambda$ and f) $h_s=6*\lambda$. The colour codes are: $\theta=0^0$ (blue), $\theta=2^0$ (green), $\theta=4^0$ (red), $\theta=6^0$ (light blue), $\theta=10^0$ (purple), $\theta=15^0$ (yellow), $\theta=20^0$ (black), $\theta=25^0$ (blue), $\theta=30^0$ (green), $\theta=35^0$ (red) and $\theta=40^0$ (light blue).

The transmission just after the blanket is shown in Figure 16 This includes also the near field components, which are not present in the plasma. The transmission increase for angles up to 20 degrees, but the beam has no power in the central position in these cases.

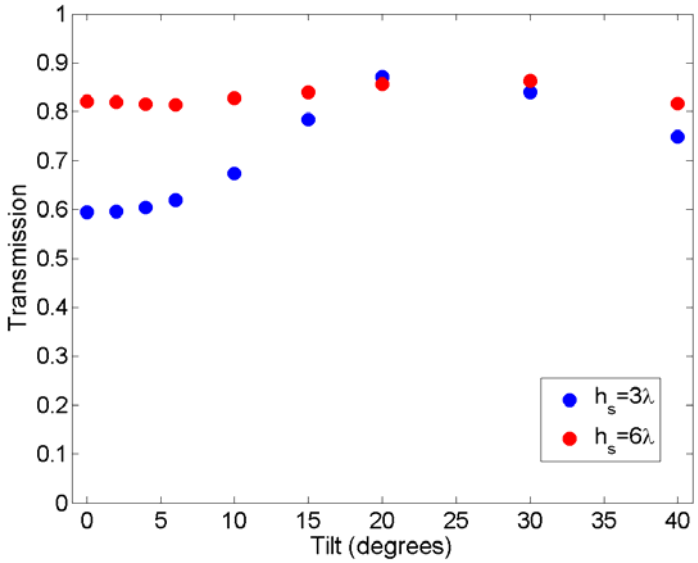

Figure 16 Transmission as a function of θ, h_s of 3*λ and 6*λ, R= 1*λ and Δ=0;

2.2.7 Conclusion from CEM calculations

Based on the results in this section where a short blanket, 20*λ, was considered. it was concluded that in order to obtain a suitable signal for the CTS measurements the following parameters should be meet; The vertical offset should be below 5 mm, which is more than the tolerances for positioning of the blanket modules. The tilt of the beam for a short blanket should be below 6^o, but for a long blanket (60* λ) this angle is scaled down by the factor (20* λ)/(60* λ) to 2^o if reflections in the slot should be limited. The radius of curvature was not so critical; it only had a small influence on the beam shape and transmission coefficient. The slot height should be as large as possible to get the lowest divergence angle and a high transmission.

3 Deliverable (ii)

Develop an improved mock-up experiment for testing front-end components:

- *Optimise the high-field-side antenna system by testing various mirrors and horn arrangements. Assess the importance of blanket edge shapes, the acceptable tolerances for positions of antenna system and blanket modules. This requires the inclusion in the mock-up of new ellipsoidally-shaped mirrors, a more-realistic blanket model, an accurate alignment/motion system for the mirrors, and a faster detection motion for the radiation-pattern measurement.*
- *Assess alignment and conditioning issues (such as robustness) on high-power transmission and receivers, including the acceptable tolerances for misalignment.*

In the following the upgraded mock-up is described in section 3.1 and the measurements in section 3.2. In section 3.3 the influence of misalignment on the scattering geometry is described.

3.1 Upgraded mock-up of the ITER CTS high field side receiver

A new mock-up of the ITER CTS high field side (HFS) receiver has been created. Due to the available mm-wave components at the Risø CTS microwave lab (Gunn oscillator, detector, waveguides, etc.) the operation frequency of the CTS transmission line for the mock-up was chosen to be 110 GHz instead of 60 GHz. Therefore, the whole geometry was scaled down by a factor of 60/110 ~ 0.5455.
The following main steps were performed to upgrade the mock-up:

- The scaled down CTS upper and lower blanket models have been produced at the Risø workshop.
- A new MatLab code has been developed allowing one to calculate (a) astigmatic Gaussian beam propagation through a given geometry and (b) the mirror surfaces used for the astigmatic beams as described under deliverable (i).

As the result, a new design of the ITER CTS HFS receiver mock-up was created (Figure 17). It should be noted that the size of the mirrors and distance between them is not like ITER, due to the used horn, which has a divergence angle of 6^{o} degrees. The two mirrors were calculated to give the right astigmatic beam at the entrance of the slot. The setup is shown in Figure 18. The system is mounted upside down to make it easy to adjust Mirror 1. Mirror 2 is fixed on the blanket. Here the cut-out to make space for mirrors and the waveguide structure between the blankets, called a slot in the following section, is also shown. The mirrors are rotated so the central beam of the 10 scattering beams hit directly on the mirrors. The extreme beams have incidence angles of up to 15 degrees.

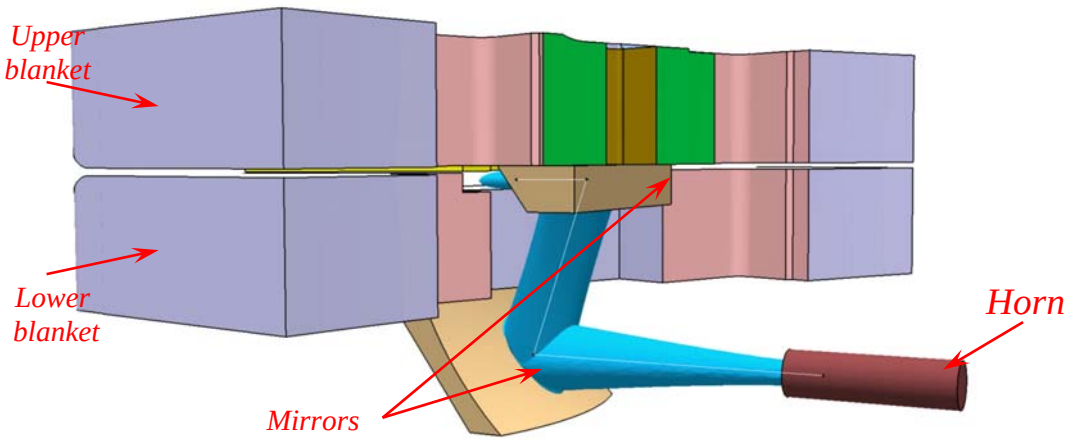

(a)

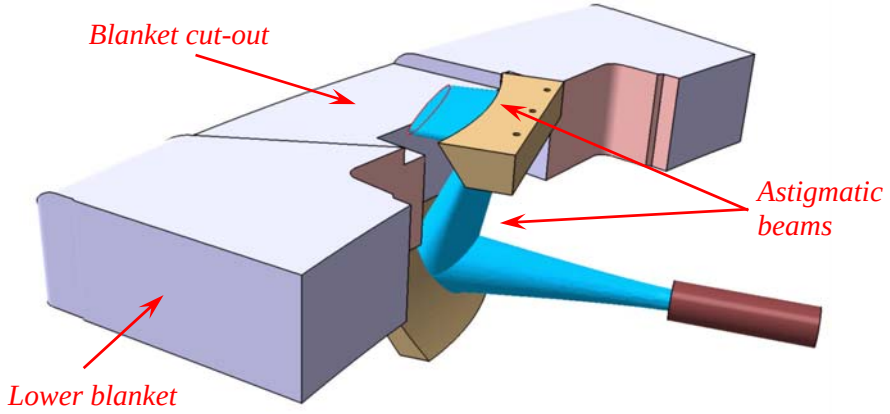

(b)

Figure 17 3D images of the upgraded mock-up of the ITER CTS HFS receiver. For visualization purposes the upper blanket is hidden in figure (b).

3.2 Mock-up measurements

In the following the measurements on an ITER mock-up are presented.
Measurements have been done to test:

- How does a change in the height of the horn influence the measured antenna pattern?
- How big a tilt of mirror 1 can be accepted?
- If it is necessary to have a spacer on the upper blanket so the beam is coming into a symmetric slot.
- How does the beam through the blanket behave as a function of distance
- If it is possible to get beams with a different angle from the last mirror through the slot i.e. measure at different scattering volume positions.

Measurements on the curvature have not been performed since there were only small differences in the calculated results. A spacer is inserted so the outcoming beam sees the same surroundings and gets a 7^{o} divergence angle. The two cases with and without the spacer inserted did not cause any considerable influence on the beam shape. The divergence angle was found in Ref. 1 to be 7^{o} for a slot height of 30 mm (60GHz).

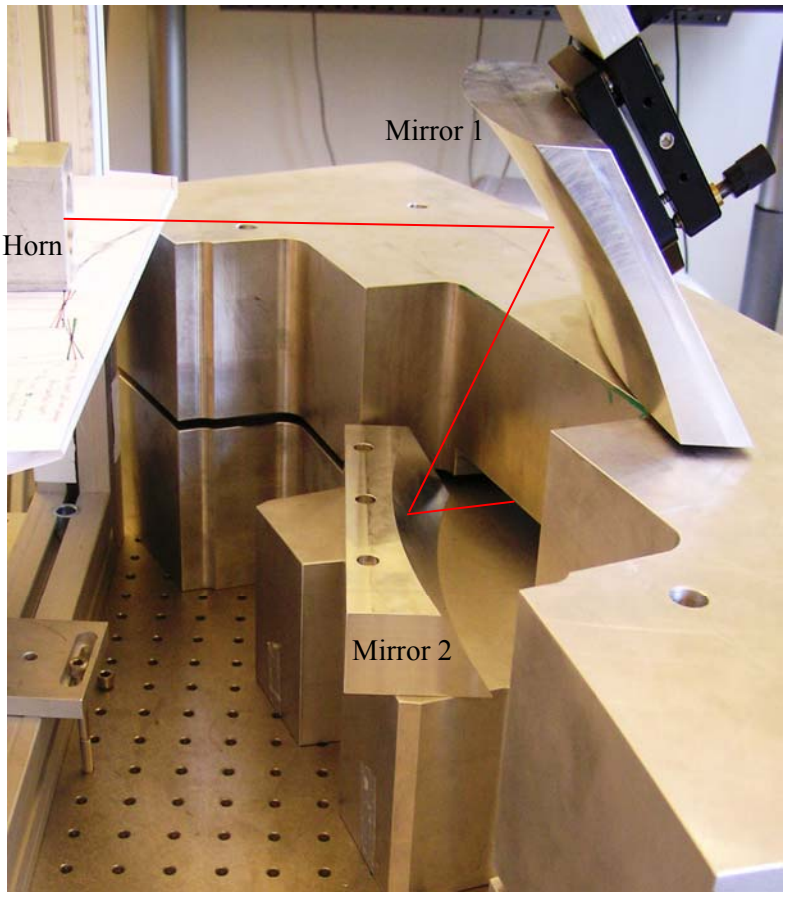

Figure 18. Set-up for measurements. The mock-up is turned up side down, to allow easy adjustment of mirrors and the horn. The red line represents the centre position of the mm-waves.

3.2.1 Change in vertical location of the horn

When the system has been aligned one parameter to investigate is the vertical position of the horn. The distance from the blanket to the detector was 101 cm (which for a 60 GHz system is equivalent to 101*11/6 cm=185 cm). It is seen from Figure 19 and Figure 20 that when the height of the horn is changed 6 mm the vertical width is changed from 7.7 cm to 6.4 cm, and the beam centre moved 12 mm up this is equal to 0.67^{o} shift of the centre. The horizontal beam width is constant and the maximum power is changed from 0.4 to 0.55 (arb. units). When the horn height is increased by an additional 5 mm, the beam has two side lopes with an intensity of approximately 10 % of the main peak as shown on Figure 21. The vertical beam width is 5.9 cm and the centre position moved 10 mm up, which is equal to a total shift of 1.2^{o}.

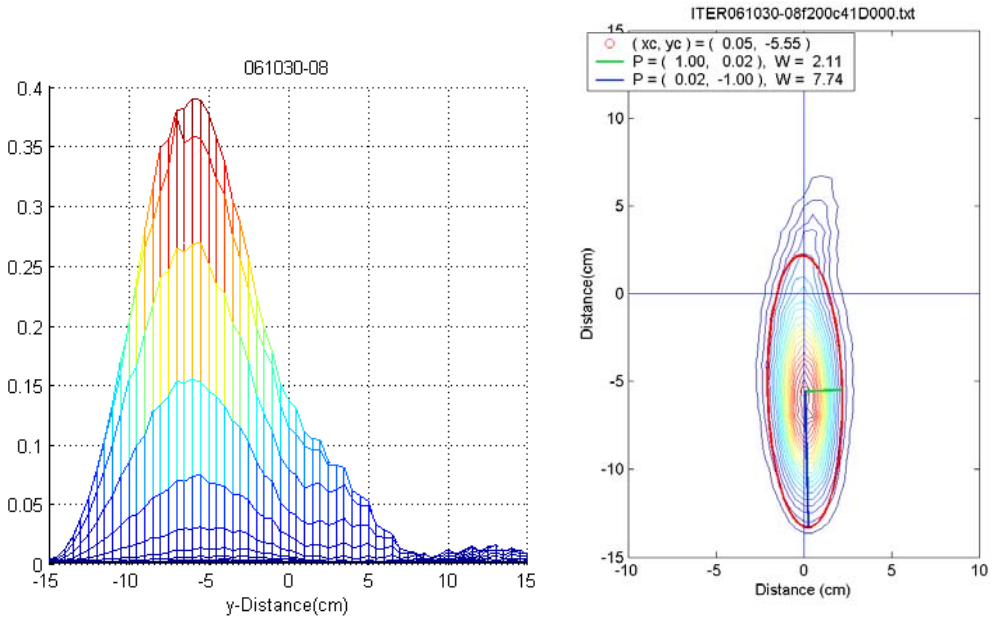

Figure 19. Vertical position of the horn: start position

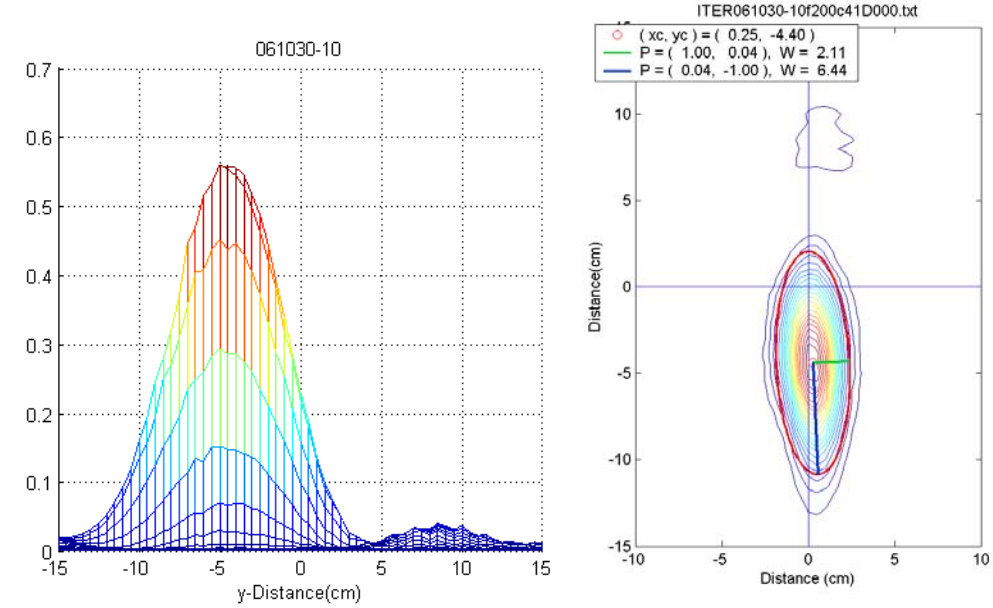

Figure 20. Vertical position of the horn: moved 6 mm in the direction away from the slot.

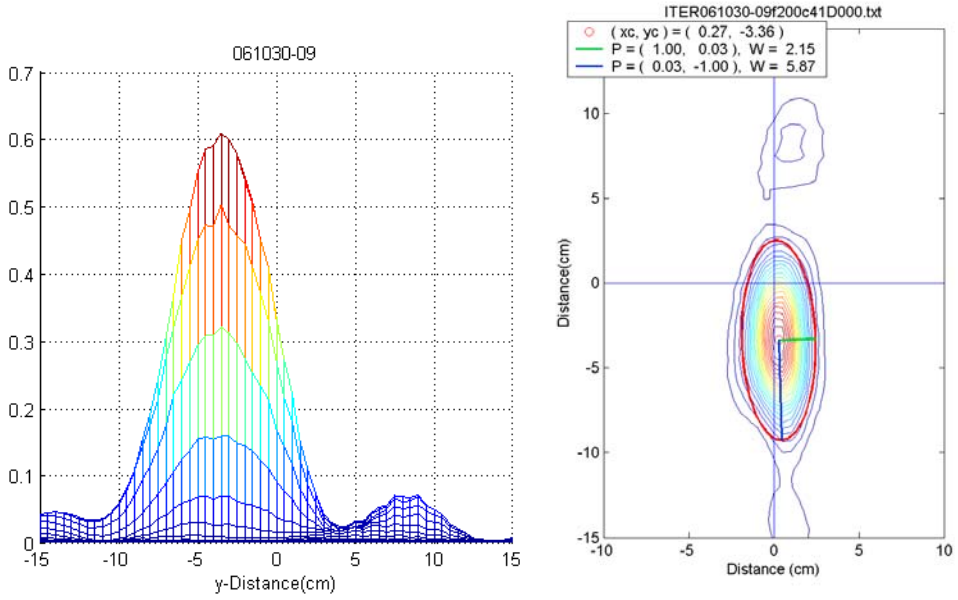

Figure 21 Position of the horn: moved 11 mm in the direction away from the slot.

It is seen that a change of 5 mm can make a change in beam profile and the centre position, therefore it is important to make the system as robust as possible. A small change in the horn position might change the centre position a little, but not much compared with the beam width, and the CTS signal will still be collected.

The measurements also show that not only does the beam centre change, the opening angle decreases where the beam width for 0, 6, and 11 mm offset has a vertical beam width (radius 1/e of E field) of 7.74, 6.44, and 5.87 cm respectively. Scattering simulations done in section 3.3 have shown that the measurement requirements are still satisfied with vertical misalignment in the output beam of less than 5 degrees. The scattering calculations have been done with the same opening angle of 7 degrees. The results from the mock-up experiments show that the opening angle is decreased with the misalignment. However, it is important to note the scattering simulations in section 3.3 assume the same amount of power in the receiver beam. There it is important that the effect of the total beam power in the main lobe is known for the misalignment studies.

3.2.2 Tilt of the beam through the blanket.

When Mirror 1 is tilted it influences the angle through the blanket. This is illustrated in Figure 22 a) and b) where the mirror is tilted 0 and 0.5˚, respectively. The reference beam comes straight through. When the mirror is tilted 0.5 degrees, the beam has a side lope which is about 1/3 of the main peak. Since it is a curved mirror a small tilt can have a large influence on the incidence angle, and the centre position of the beam on the second mirror. This will give rise to another offset and angle at the entrance of the slot, which can cause side lopes if the beam hits a side of the cut-out.

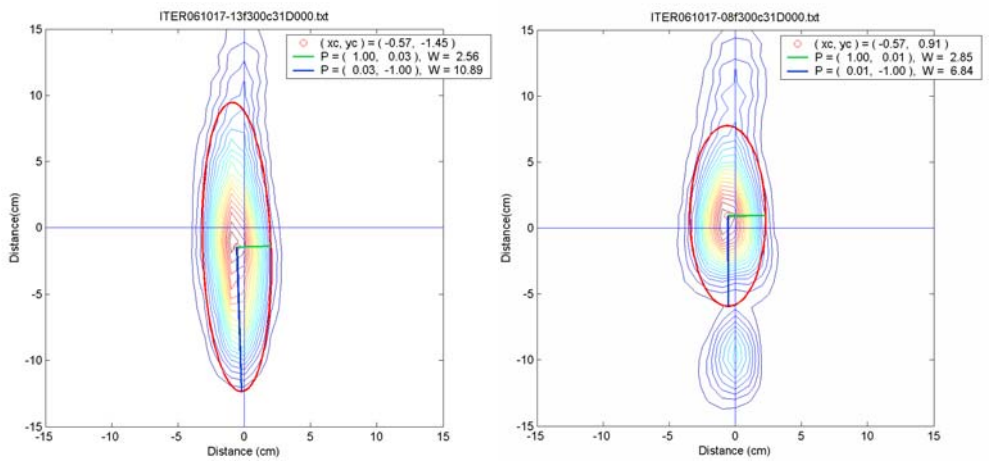

Figure 22. L=60.5 cm. a) start and b) 0.5˚ tilt

3.2.3 Test of the spacer inserted in the blanket

When there is a cut-out of the blanket to give room to the mirrors, the beam might not see the same surroundings when it comes out of the slot, since the position of the mirror is limited by the blanket key. To let the beam experience a divergence angle of 7 degrees both up and down, an extra spacer can be added on one blanket as illustrated in Figure 23 and Figure 24 to displace the beam down. The height from the spacer to the other blanket is h_s=16.5 mm=6*λ (in 60 GHz frame is this 30 mm). Investigations of the effect of the added spacer have been done. When the spacer is not included the height is 21mm and the beam is misaligned by 2 mm with respect to the centre of the slot.

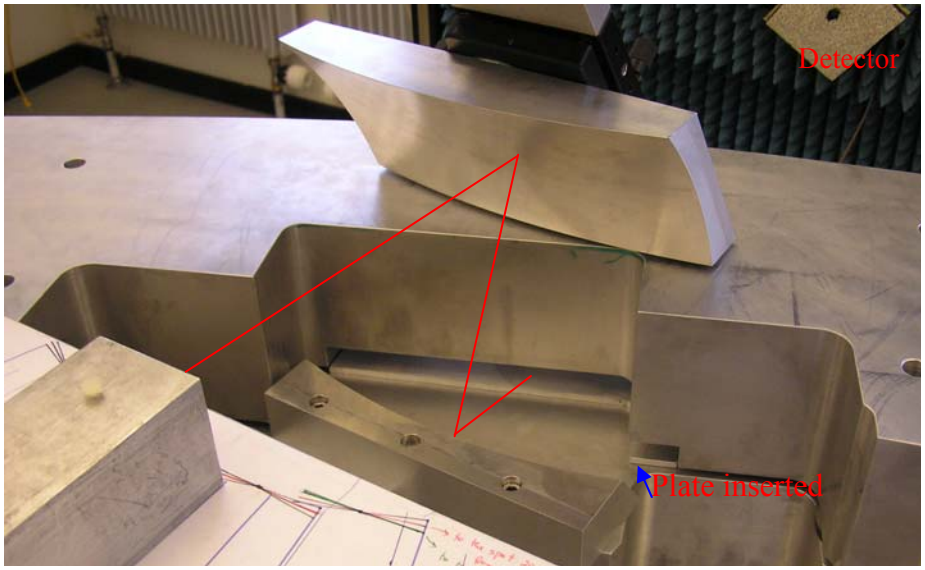

Figure 23. Setup for testing the influence of a spacer added on the blanket (the upper one, on ITER)

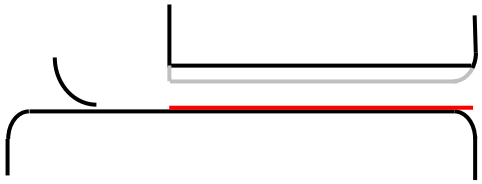

Figure 24. Illustration of the blanket with the spacer inserted. The grey areas represent the removed part of the blanket. The red line is the inserted spacer.

The spacer does not influence the centre beam much as illustrated on Figure 25 and Figure 26, without and with a spacer,, respectively. It has a tendency to make the beam narrower. This was expected since the mirrors are designed for the case with the spacer inserted, where the beam centre is shifted a bit compared with the case with out the spacer. Note that the spacer is giving the same length on the upper and lower blanket (as seen on Figure 24). This means that the results of measurements are a combination of curvature and the spacer, and they do not influence the beam significantly.

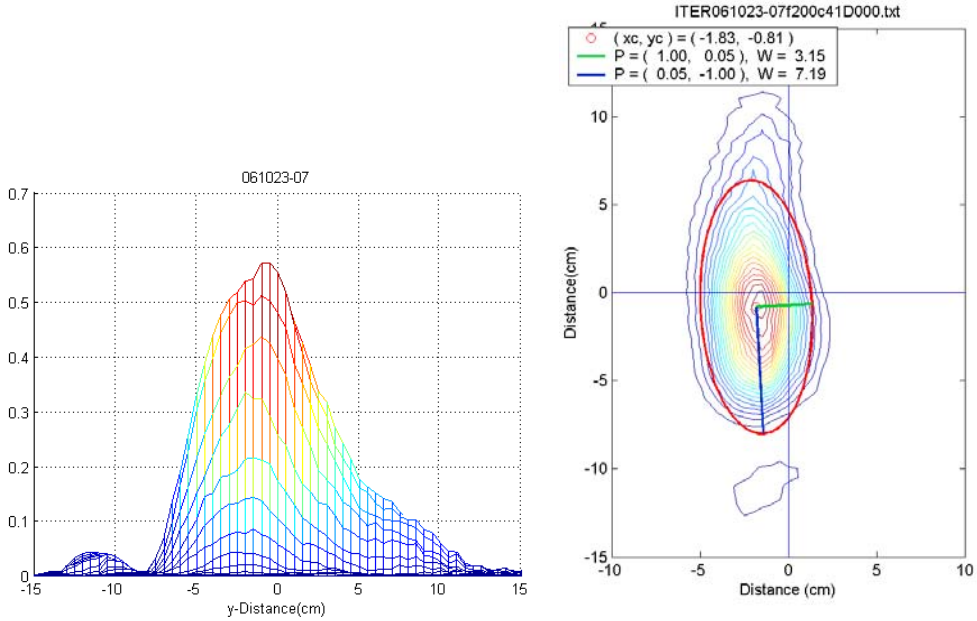

Figure 25. Beam pattern after the blankets without the spacer.

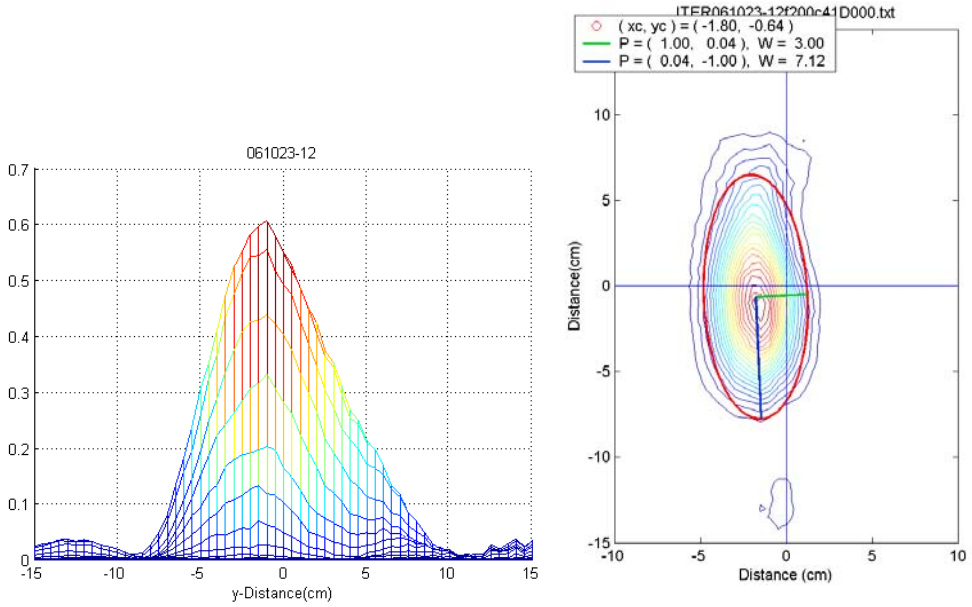

Figure 26. Beam pattern after the blankets with the spacer.

3.2.4 Beam width dependence on the spacer

To investigate how the beam propagates from the slot, the antenna pattern was measured in different distances from the blanket. The data has been fitted to the expression for a Gaussian beam width,

$W = W_0\sqrt{1+\left(\frac{(z-z_0)\lambda}{\pi W_0^2}\right)^2}$ to get the beam waist position (z_0) and width (W_0). The divergence angle is given by: $\theta = \frac{\lambda}{\pi W_0}$ and it is quoted in degrees.

It is seen in Figure 27 that the beam with and divergence angle are not affected by the spacer. The position is changed a little, but within the error-bars. Note that when the spacer is not inserted the height is 21 mm, and the divergence angle becomes smaller. The blue curves shows the expected curves based on the values from calculations which are $W_0(x)$=22.1 mm, $Z_0(x)$=1130 mm, $W_0(y)$=7.1 mm and $Z_0(y)$=64.5 mm. It is seen that the measured data derivate from the expected curves.

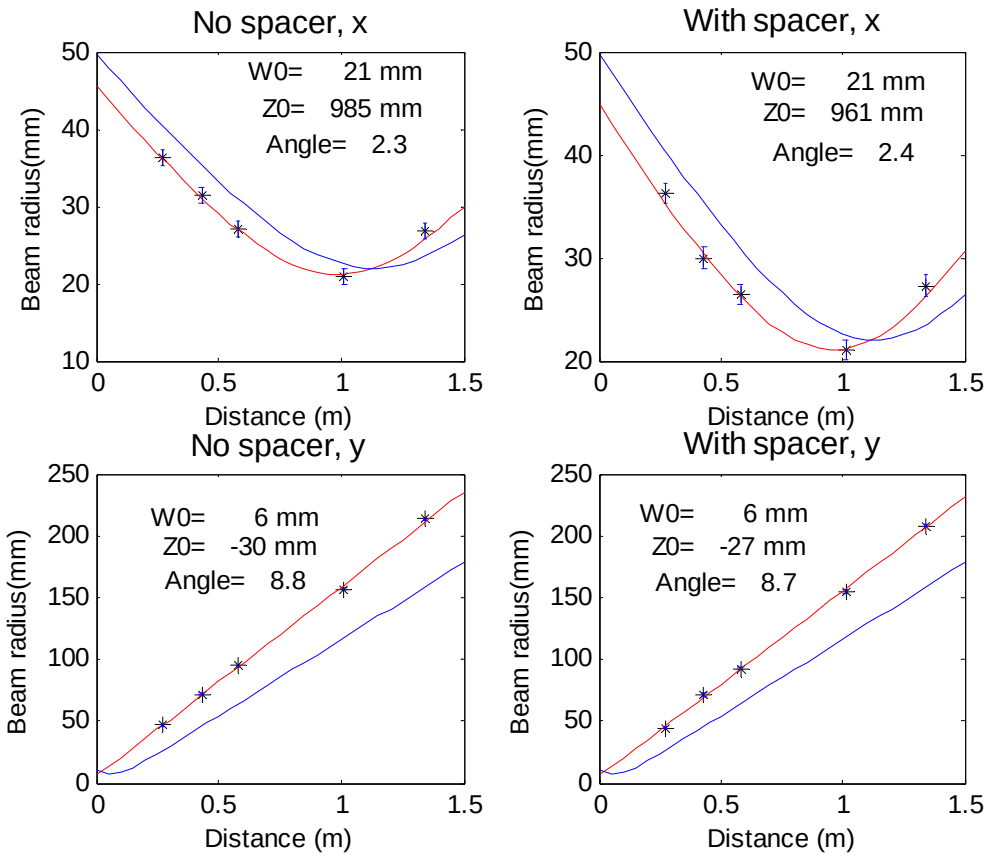

Figure 27. Properties of the beam width without spacer and with spacer

When the height of the beam is changed by 3 mm the results are as shown on Figure 28. The blue curve is the expected and the red the found curves. It is seen that the beam waist (W_0) and the angle are not affected in the x direction, but the position (z_0) is moved about 10 cm compared with the previous results. In the y-direction the spacer has a larger influence on the position and a bit on the angle. It is seen that in the case with the spacer the divergence angle is smallest, which is expected due to the smallest slot height.

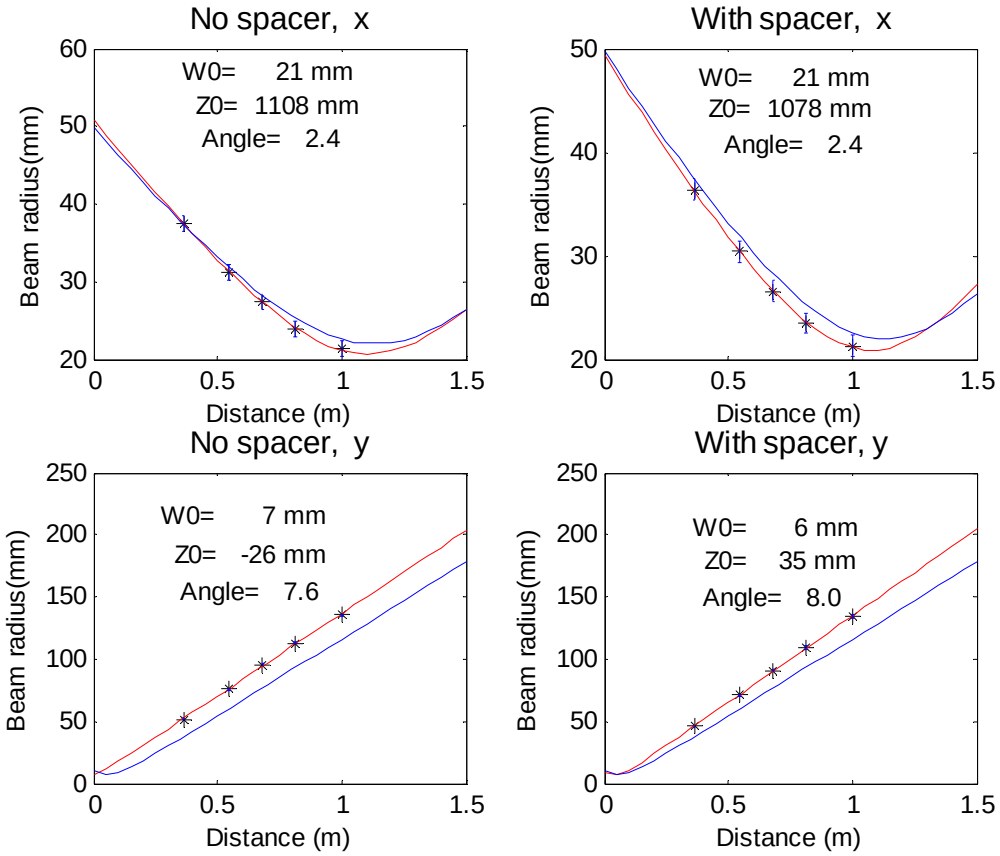

Figure 28 Properties of beam width for an increased horn position and with and without the spacer.

3.2.5 Investigation of different beam angles from the slot

At the HFS it should be possible to measure the scattered light from 10 different scattering volumes. The beam hits the first mirror (from the plasma) under different angles, but with the same horizontal size. This is illustrated in Figure 29, where the green beam gives an output angle of 15^0 and the blue beam gives an output of -15^0 with respect to the centre beam.

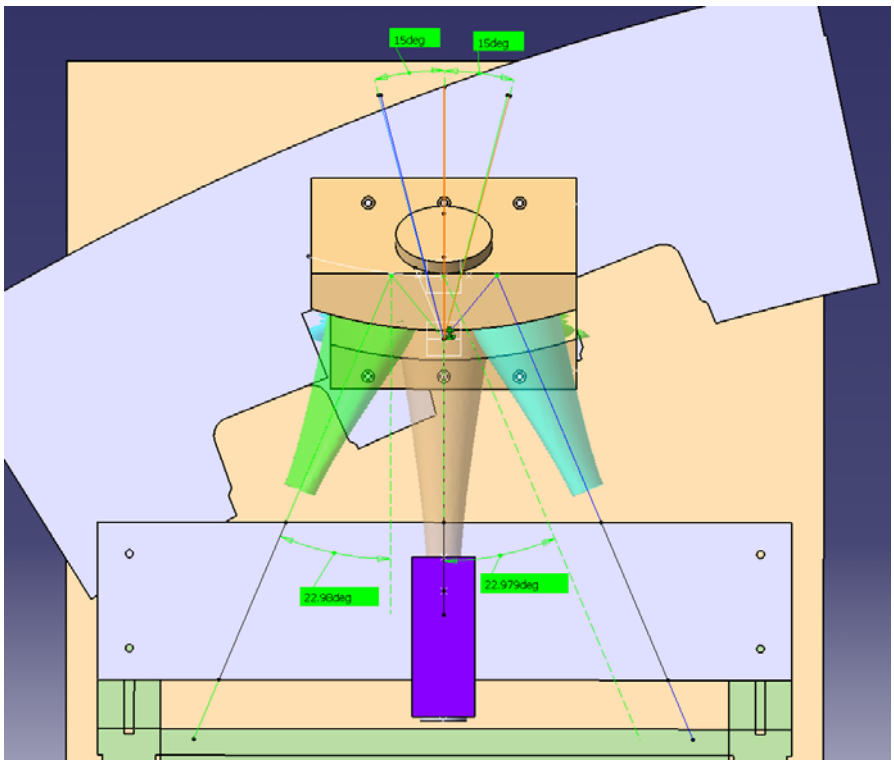

Figure 29. Illustration of different position of beams, to get outputs with angles +15 and -15 degrees for the green (left) and blue (right) beam, respectively.

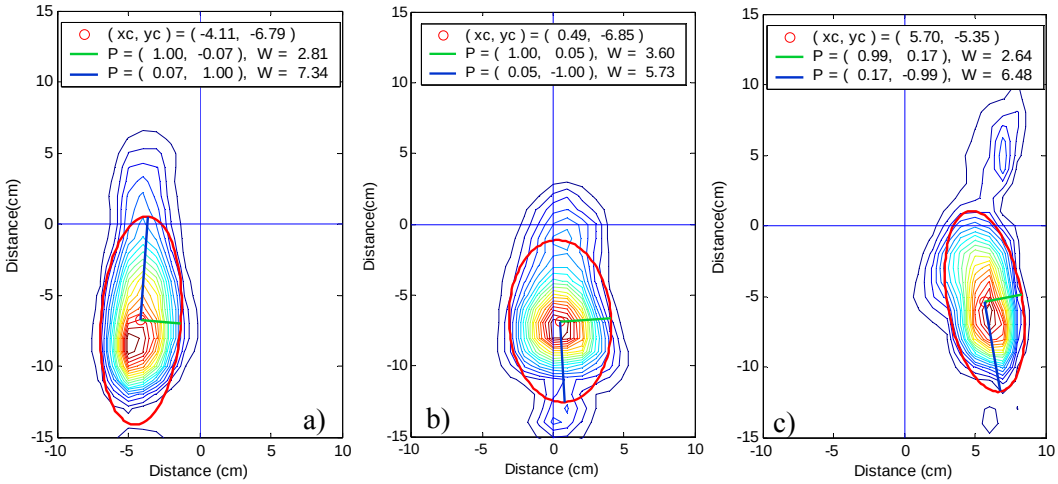

Figure 30. Antenna pattern for a) right angle incidence, the beam is displaced 14.1 cm to the left, b) centre beam, c) left angle, the beam is displaced 15.7 cm to the right.

It is seen that from Figure 30 that two extreme beams can propagate through the slot. The power in the centre beam is about 0.75 in arbitrary units at this distance (L=38 cm), the two extreme beams has power loss of about 50 percent for left and right beams, respectively. The distance is chosen so the left and right extreme beams can be measured with the same detector setup. The two beams have out coming angles of 15 and 14 degrees for left and right extreme beams, respectively, which is in excellent agreement with the expected angles of 15 degrees. It is seen that the two extreme beams are tilted, which is due to the non-optimal curvature on the mirrors for these beams. Further investigations of different angles will be performed when a 4-mirror system is produced.

3.2.6 Conclusion

Alignment of the mirrors was investigated in this section. It was found that the horn position can be changed a few mm without significant loss of beam power; it mainly changed the beam shape. The tilting of the mirror has a larger influence, so it should be small to prevent side lopes and displacement of the central peak. The actual angle tilt through the slot was difficult to estimate from these measurements.
It was also shown that it was possible to collect the scattered signal at the extreme angles, but in these cases the maximal power decreased to about 50 %. This should be investigated further when a 4-mirror system is produced.

3.3 Scattering calculations

A misaligned receiver beam can propagate through the slot as illustrated in the previous sections, but the scattering volume might be different. In the following section the influence on the scattering calculations of misalignment is presented.
In the physics feasibility and physics conceptual design studies [Ref. 1], the choice of scattering geometry was optimised. The optimisations are primarily driven by the need to satisfy requirements on; resolving power, spatial resolution, and robustness all at a broad range of plasma parameters. The resolving power was defined and discussed in Ref. 1 section 1.8. It is a measure of the accuracy with which the system can estimate the fast ion velocity distribution for a given velocity space resolution. For all systems discussed in this report, a minimum resolving power of 4 is selected. This corresponds to requiring that the systems resolve at least $L^2 = 16$ orthogonal components of the fast ion velocity distribution, essentially points in, the fast ion distribution, with an uncertainty, σ, smaller than the target accuracy, $\Delta = 6\times10^9 s/m^4$.

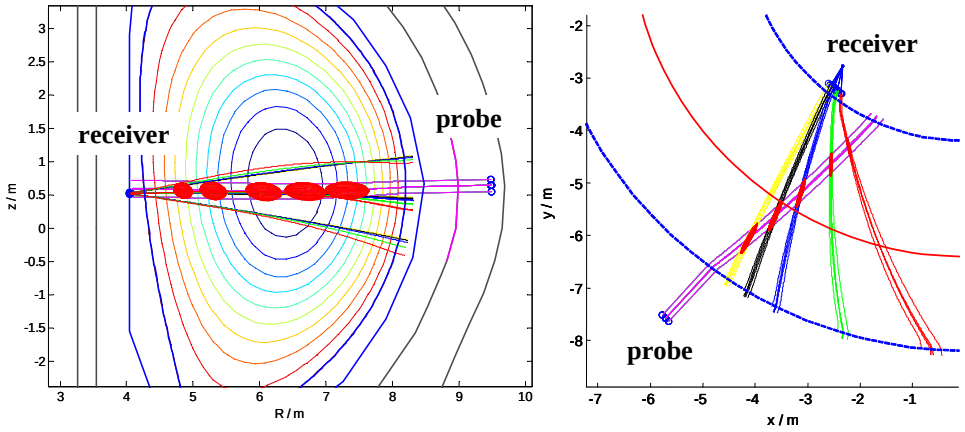

Figure 31. HFS-FS scattering layout viewed in the poloidal plane (a) and viewed from the top (b). Five receiver beams are shown where the yellow and red are the extreme beams. The opening angle is about 30°. Also shown are the red ellipsoids that represent the scattering volume (90% of the total scattering radiation).

Optimisations included choice of scattering angles and choice of Gaussian beams for the probe and receiver within the engineering constraints imposed by ITER. The poloidal view of the scattering geometry of the HFS-FS system is shown in Figure 31(a). The receiver views the plasma from a gap between the HFS blankets. The beams from the receiver diverge in the vertical direction, as illustrated by the 2 lines

representing the Gaussian half widths. The top view of the HFS-FS system in Figure 31(b) also shows the receiver viewing angle of 30°. This corresponds to a plasma coverage of ρ between -0.5 (HFS) and 0.5 (LFS) if the centre beam (normal to the first mirror) is viewing the centre of the plasma.

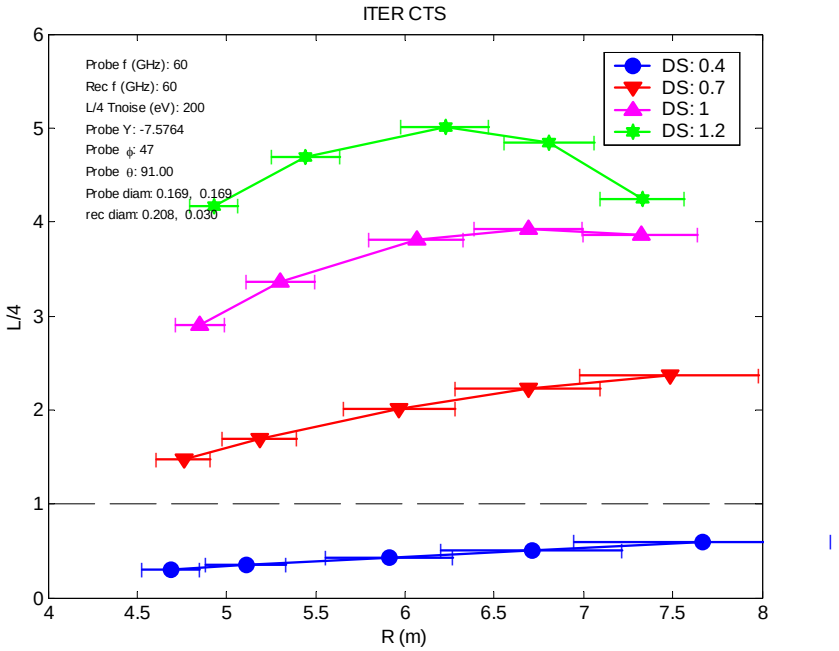

Figure 32. Resolving power, L/4, of the CTS HFS-FS system for the fusion alphas against the radial location of the scattering volume. Each colour and symbol represents a plasma density by scaling reference plasma density by the factor DS where DS = 1 = $n_e(0) = 1.0 \times 10^{20}$ m^{-3}.

Scattering calculations results in Figure 32 show the robustness of the system to a density range between 0.5 – 1.2 $\times 10^{20}$ m^{-3}. The CTS ITER reports [Ref. 1] have shown that the present design is robust against variations in plasma parameters and dispersion effects. In addition, studies of different plasma scenarios have also been reported and have concluded that the largest affect on the diagnostic performance is the plasma density. However, minor misalignments of the system are expected in a harsh environment such as the operating burn scenario of ITER.

3.3.1 Vertical misalignment of the probe beam

This section will cover the effect of the scattering simulations against misalignments in the first mirrors of the probe and receiver. Before continuing on the subject, it is important to note what is affected exactly for both vertical and horizontal beam properties of the system. The *beam plane* is the plane that includes the centre of the scattering volume and is spanned by the direction vectors of the two beams. For the HFS-FS system, the beam plane is on the horizontal axis. Beam properties perpendicular to the beam plane, hence vertical for the HFS-FS, affects the CTS signal [Annex 2 of Ref 1]. The beam properties parallel to the beam plane will mainly affect the spatial resolution. Viewing the poloidal cross section in Figure 31, one can see that a vertical misalignment of either the probe or receiver will mainly affect the measurements on the HFS.

This is what is observed in Figure 33 where the vertical launching angle of the probe is changed. The figure also shows that the maximum signal is attained when the probe beam is about 1° above. This is due to the effect of the poloidal magnetic field that causes the beam to propagate downward. Figure 33 also shows the minimum amount of the vertical misalignment that will still satisfy the measurement requirement ($L/4 \geq 1$) for each radial location. Thus for the centre measurement in the plasma at DS = 1.0, the probe should not be misaligned more than -2°. In these simulations the beam properties are kept the same and a 1 MW power is assumed. Hence changes in the beam property or the beam power are not taken into account in these simulations.

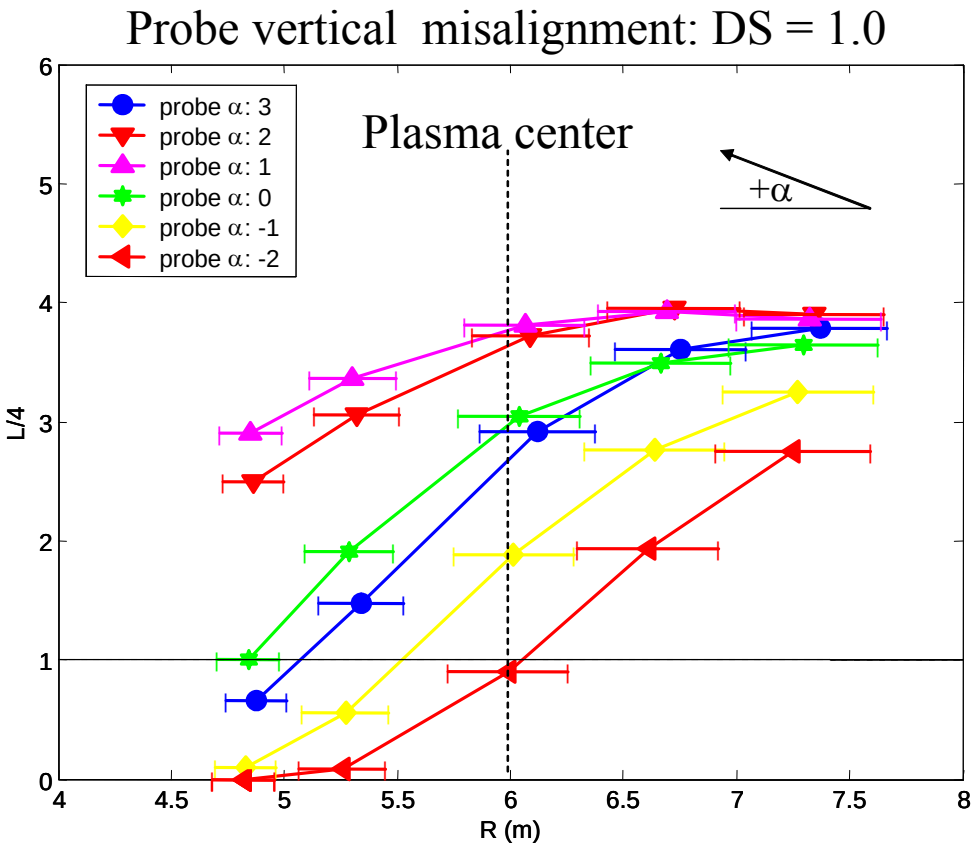

Figure 33. Resolving power L/4 for density scaling DS = 1 for different vertical misalignment of the probe where α the angle from the horizontal axis.

Not shown is the same graph for DS = 0.7 and for DS = 1.2 where the vertical misalignment limit for the center of the plasma measurement is -1° and -2.5 ° respectively. The measurement of the plasma surface ρ is not affected greatly by the vertical misalignment of the probe.

3.3.2 Vertical misalignment of the receiver beam.

Any misalignment with the first mirror to the blanket slot will cause the incident angle to change. Sensitivity studies of the misalignment in the mock up calculations (section2.2.6) have shown that angles up to 2˚ can be given. In this section the effect of the changes of the elevation angle of the receiver beam is verified. It is important to note that in these simulations, the beam properties are kept the same, i.e. the beam

divergence and the horizontal beam properties the same. In addition, it is also assumed that the beam in the simulations have 100% of the power. Therefore there are no main side lobes. It is simple to calculate the reduction of the CTS signal from the reduction of the main lobe due to the fact that the resolving power is directly proportional to the beam total radiation power.

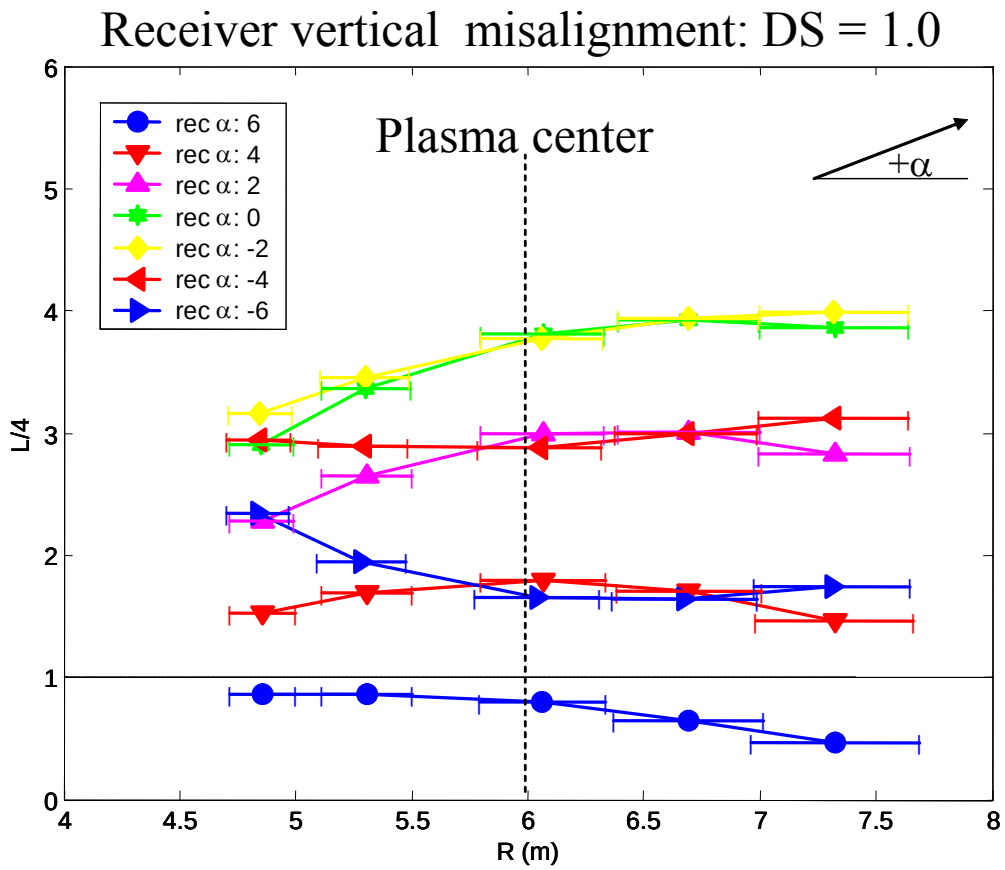

Figure 34. Resolving power, L/4, for plasma density scaling of DS = 1 for different elevation angles (α) of the receiver where α = 0 is horizontal.

From the simulation result shown in Figure 34, the CTS signal is much less sensitive to vertical misalignment of the receiver. The range where the entire measurements still satisfy the measurement requirements for elevation between to +5 to -7° compared to -2° for the probe. The reason for this is the expanding beam of the receiver results in CTS measurements on the LFS that are less sensitive to vertical displacement compared to HFS measurements. Obviously, probe vertical misalignment will cause largest displacements in the more sensitive region compared to the receiver vertical displacements where the largest displacement is on the less sensitive region (LFS).

3.3.3 Horizontal misalignment of the probe beam

The horizontal launch direction will affect the scattering angle. This will in turn affect the CTS signal and the spatial resolution. The smaller the scattering angle the larger the overlap which is directly proportional to the resolving power. However, a smaller scattering angle will lead to a longer scattering volume; hence the radial resolution will be lower.

The simulations performed in the previous section were for horizontal launch angles of +6° to the right from pure radial. Figure 35 shows the scattering simulation results for angles +/- 4 degrees from this reference point.

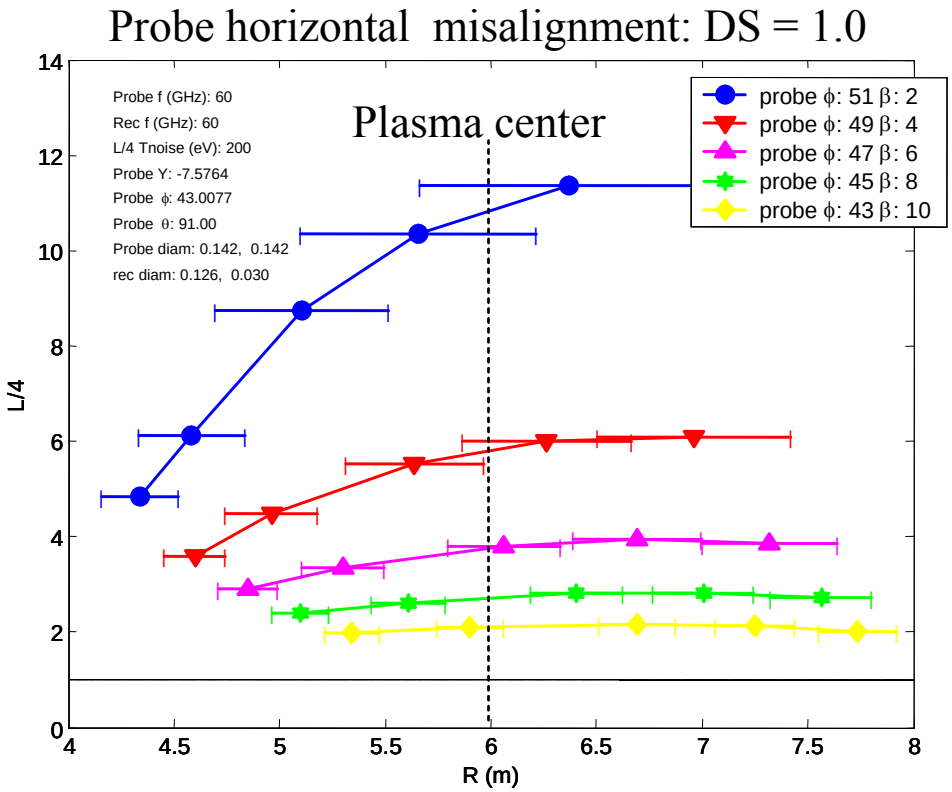

Figure 35. Resolving power L/4 vs. Radial position for different horizontal launch angles where β = is pure radial and positive is to the right viewing from the launching mirror.

The reader can notice the compromise between CTS signal and radial resolution. Any misalignment within 4° from the reference angle still satisfies the ITER requirements for the fusion alphas. With the possibility of remote steering, the system will have the added flexibility in increasing either increasing the CTS signal or increasing the radial resolution for different plasma parameters.

3.3.4 Horizontal misalignment of the receiver beam

The horizontal misalignment of the receiver has some effect on the CTS signal. However according to the scattering simulations shown in Figure 36, the measurement requirements are still satisfied for a horizontal angle misalignment in the receiver beam of 6˚.

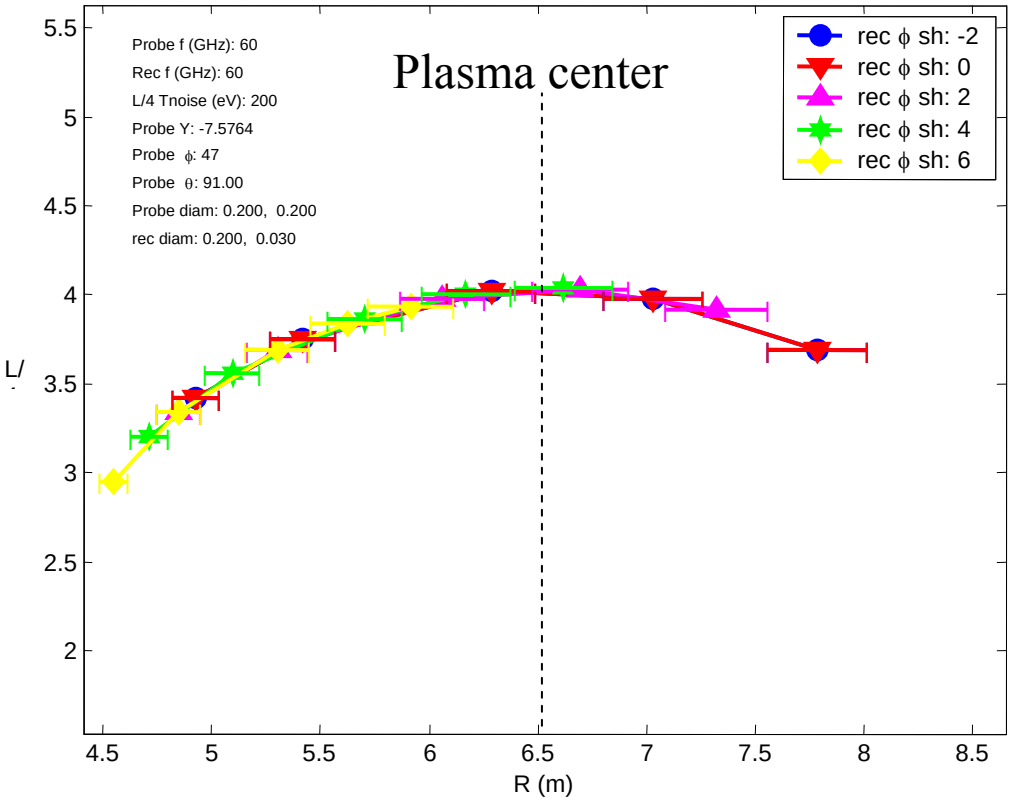

Figure 36. Resolving power L/6 vs radial location of the measurement for different horizontal angle. The reference angle is the red upside down triangle.

3.3.5 Conclusion

It was found that the probe is the most critical component, since it could be moved only 2˚ in the vertical direction and 4° in the horizontal direction. By the cut-out in the blanket, the receiver beams are limited to 6° in the horizontal direction and between -5° -7° in the vertical direction. The angle in the vertical direction is much smaller due to the slot, if reflections on the blankets should be prevented as shown in section 2.2.6. Here it was found that the angle should be below 2°.

4 Deliverable (iii)

Study key mm-wave components, and other critical components and issues:

- *Investigate the relative merits of circular and rectangular horns for the receivers.*
- *Optimize the mirrors for transmission of beams from a set of horns.*

4.1 Investigation of horns

If it is not possible to produce a circular beam at the horn antenna position with the optical beam path available, receiving an elliptical beam with a rectangular horn is a possibility. The output from this horn depends on the relationship between the two horb sides. The normal rectangular horns are designed to give circular beams. The drawback of rectangular horns is the polarization dependence, since our signal might not have the polarization in the same direction as the smallest Gaussian width. The circular horns are not dependent on the polarization. The 4-mirror solution described in the next section transforms an astigmatic beam into a circular Gaussian beam, making it possible to use circular horns.

4.2 CTS diagnostic on the high field side (HFS)

For the CTS HFS receiver, a slot of approximately 350 x 30 mm in the blanket should be available. A beam with a high ellipticity travelling through this slot needs to be converted to a small symmetrical beam with small ellipticity suitable for a symmetrical horn antenna. Avoiding mirrors with excessive curvature requires a long travel path for beams with large spatial extension, which shall be focused to a small horn. This is the case for the horizontal extension of the beam (Gaussian radius: 0.1 m at the slot). Since the vertical extension of the beam (9.4 mm) is smaller than the horizontal one, the beam would diverge in the vertical direction along the travel path. This difficulty can be overcome by using 4-mirrors instead of 2. A 2 mirror case has been described in Ref. 2. The resulting long travel path allows the horizontal extension to be focused to a small radius of 4.5 mm, while the 2 additional mirrors allow refocusing the beam in the vertical plane. The beam propagation was calculated in Matlab. In order to catch more than 99% of the beam power, the opening size should be at least 1.6 times the Gaussian width. (A Gaussian beam with the radii 100 and 9.4 mm require a slot of 320mm x 30 mm)
Figure 37 shows the beam radii in the vertical and horizontal direction versus the travel path after it passed the slot in the blanket. The green circles in the graph indicate the position of the mirrors. The blue circle is the position of the horn antenna.

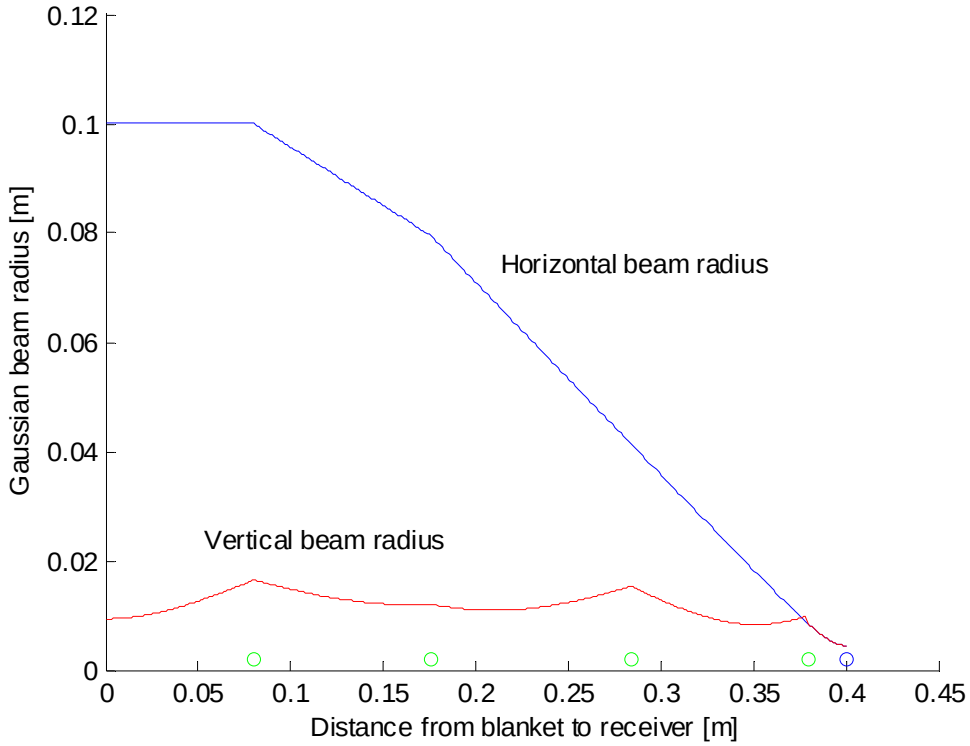

Figure 37: Vertical (red) and horizontal (blue) beam radius along the travel path from the inner edge of the blanket to the detector. The green circles indicate mirror positions. The blue circle is the detector location.

The beam propagation from the plasma volume to the slot in the blanket is shown in Figure 38. The slot of the blanket is positioned at 0 on the x-axis.

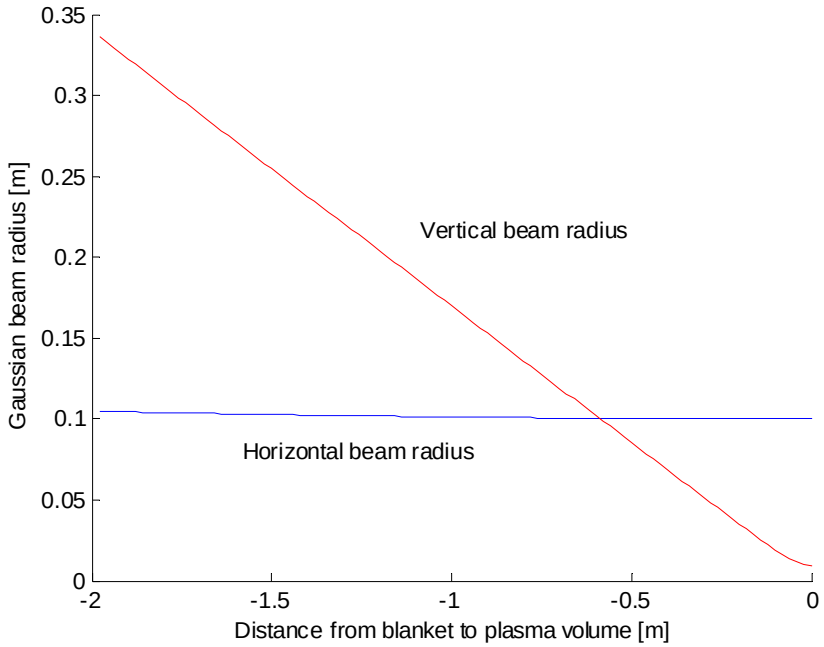

Figure 38 Vertical (blue) and horizontal (red) beam radius along the travel path from the plasma to the outer edge of the blanket. The blanket starts at position 0.

In a distance of 2 m from the blanket the Gaussian beam width is 1.12 m x 0.35 m (= radius x 2 x 1.6)

The mirror shapes are also calculated in MatLab using the astigmatic code described in section 2.1.2. The data are imported into CATIA, where the mirrors are designed. Figure 39 shows the 4-mirror assembly. The geometry is designed so that radiation from 15˚ off centre can also be detected. The central beam profile is shown in Figure 39. The red lines indicate the optical axis of the beams +/- 15˚ from centre and at centre.

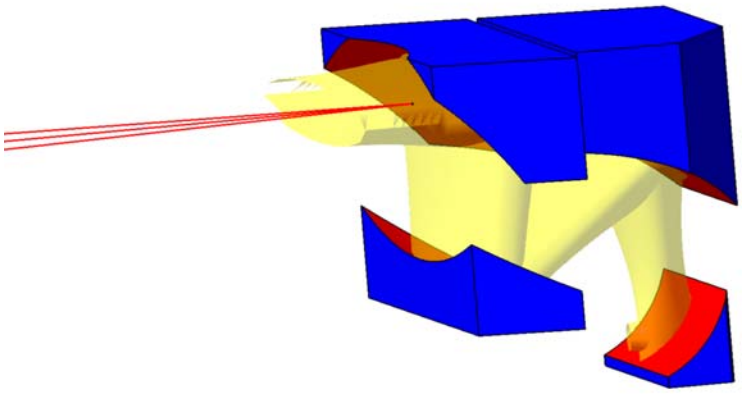

Figure 39: Mirror assembly to focus the elliptical beam at the slot in the blanket to a circular beam at the horn. The horn is not shown in the figure.

Figure 40 shows the mirror assembly integrated in the tokamak. The upper blanket is hidden. The receiver is supposed to detect radiation between 7˚ and 37˚ relative to the radial axis. Therefore the assembly is turned 22˚ relative to the radial direction.

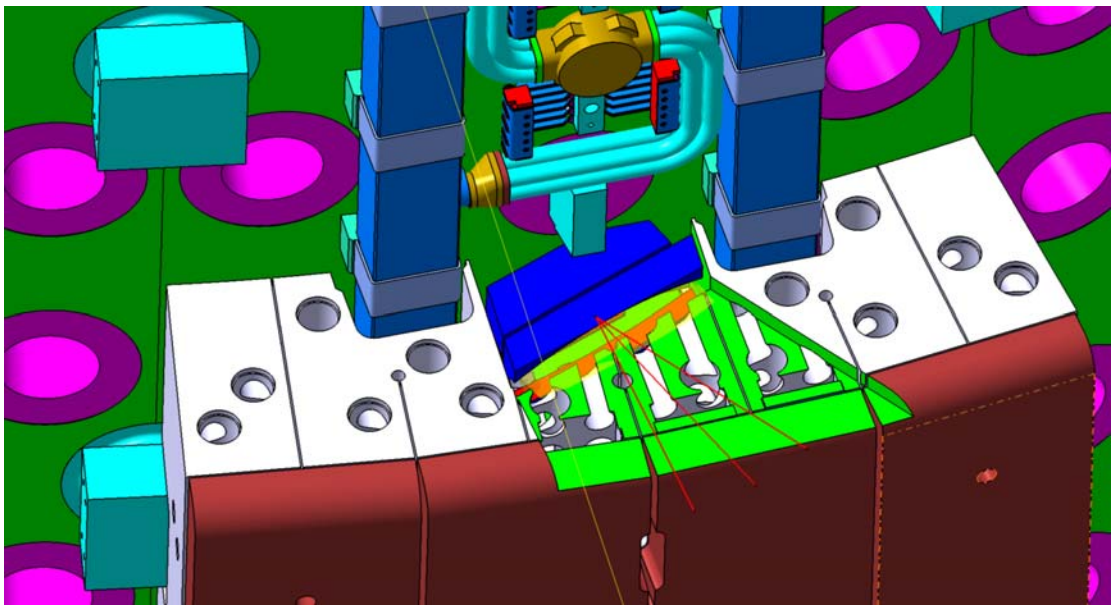

Figure 40: Mirror assembly integrated between blanket and wall of the Tokamak

Figure 41 shows the slot between the upper and lower blanket. The vertical cut is 30 mm. A spacer (10 mm) is placed underneath the upper blanket.

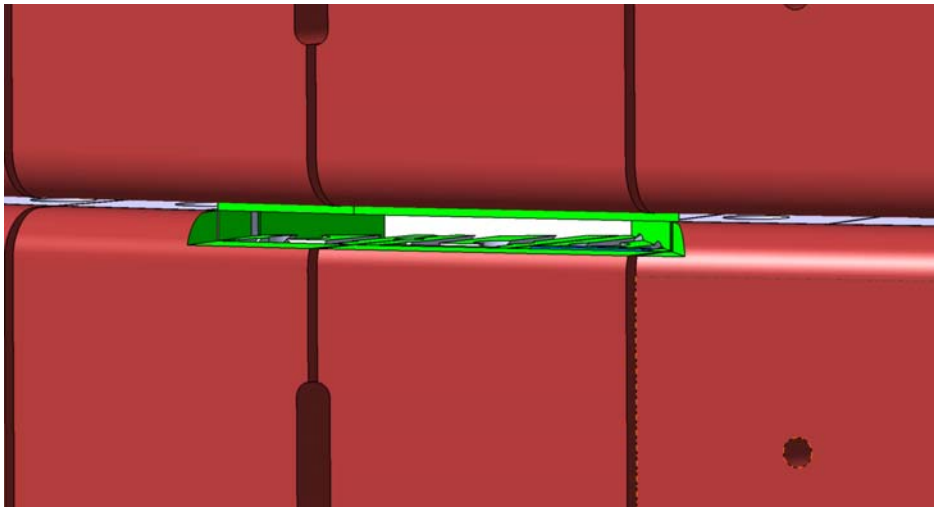

Figure 41: Front view of the slot in the blanket for the CTS HFS receiver

The backside of the blanket is shown in Figure 42. It shows the cut-out requirement for the diagnostic. The height of the cut-out is 190 mm. It is limited on top by a key and at the bottom by a supply pipe. This space is required to fit in the mirror assembly.

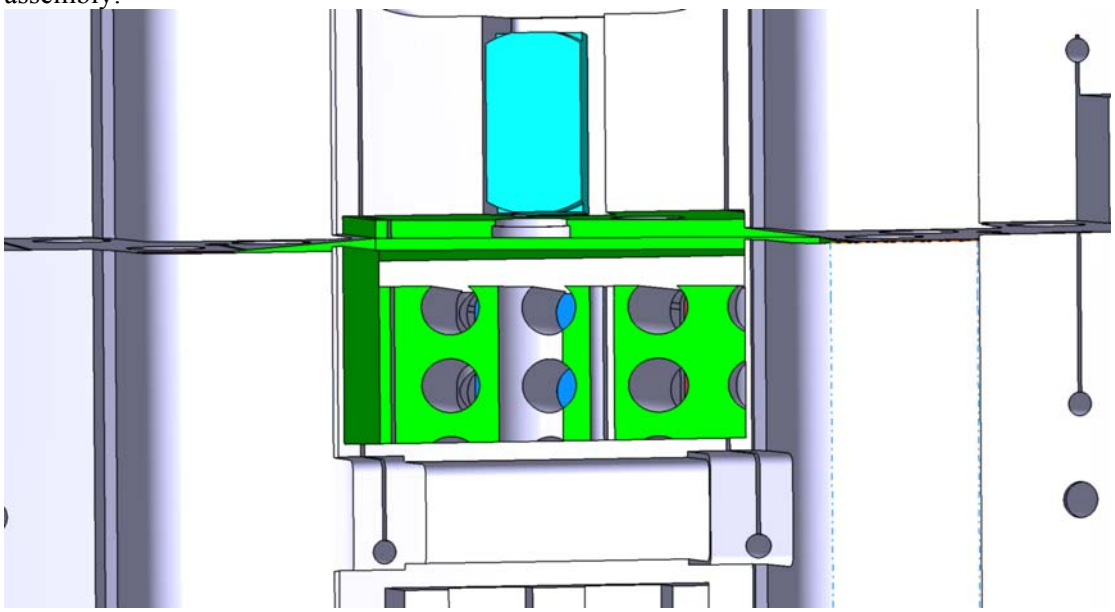

Figure 42: Back view of the blanket. The pocket needed to be cut out is shown in green.

Figure 43 shows a sketch with the dimensions of the cut-out.

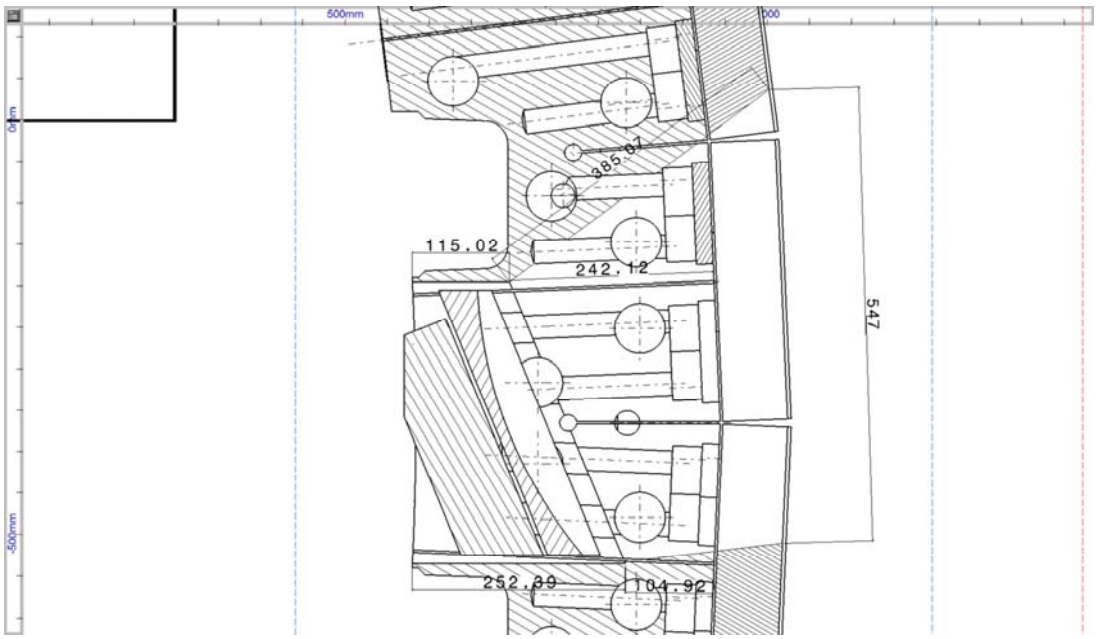

Figure 43: Top view of blanket: Sketch and dimensions of cut-out

4.3 Conclusion

By producing a 4-mirror antenna it is possible to get circular beams at the horns, and it is therefore optimal to use circular horns. The mirrors are inserted with an angle to get the beam from the central scattering volume at normal incidence on the first mirror. The cut-out is also angled so it is minimized.

5 Discussion and Conclusion

New codes for calculation of 3D mirrors for astigmatic beams have been developed. The shape of the beam for a 2 or 4-mirror system can be calculated. Thus it is possible to calculate horn positions for all scattering volumes on the HFS.
A new set of mirrors have been produced and tested with a horn antenna with a divergence angle of 6^0. On ITER HFS there is not space for a long horn so horns with higher divergence angles have to be used. Mock-up measurements showed that the horn could be misaligned about 3 mm without any significant change of antenna pattern. A small tilt of the mirror may be more critical. A tilt below 2 degrees seems however to be acceptable according to the CEM calculations. This has to be investigated more when a 4-mirror antenna system is produced. The calculations on misalignment influence on scattering geometry showed that alignment of the probe was more critical than the receiver alignment on the HFS.
It was finally shown that a 4-mirror antenna system on the HFS makes it possible to use circular horns.

6 IPR

The tasks performed and described in this report are: 1) Optimisation of the design, considering the scattering geometries, variations in plasma profiles, magnetic equilibria etc. 2) Development of numerical codes for determination of the geometry of the antenna system on the high field side, including shapes and positions of mirrors and receiver horns. 3) A model experiment was set up in order to test and support the theoretical and numerical results. The software used was either developed specifically to this project, or developed as part of the EFDA tasks presented in Ref.: [1, 2].

Based on the description above we conclude that the relevant background IPR used in this contract was generated during execution of former work supported by EFDA and the Commission. The developed software for propagation of electromagnetic waves can be considered as part of the ITM agreement. However these calculations could probably also have been done with commercial software. The results and the report are protected by intellectual property rights. The authors conclude that no further foreground IPR worth protecting has been generated under this contract.

7 References

1. H. Bindslev, F. Meo, S. Korsholm, ITER Fast Ion Collective Thomson Scattering, Feasibility study (EFDA Contract 01.654)

2. Henrik Bindslev, Axel W. Larsen, Fernando Meo, Poul K. Michelsen, Susanne Michelsen, Anders H. Nielsen, Søren Nimb, Erekle Tsakadze, ITER Fast Ion Collective Thomson Scattering, (EFDA Contract 04-1213)

Risø DTU is the National Laboratory for Sustainable Energy. Our research focuses on development of energy technologies and systems with minimal effect on climate, and contributes to innovation, education and policy. Risø has large experimental facilities and interdisciplinary research environments, and includes the national centre for nuclear technologies.

Risø DTU
National Laboratory for Sustainable Energy
Technical University of Denmark

Frederiksborgvej 399
PO Box 49
DK-4000 Roskilde
Denmark
Phone +45 4677 4677
Fax +45 4677 5688

www.risoe.dtu.dk